Supplementary Materials for

Synthesis and Luminescence Properties of Two-Electron Bimetallic Cu-Ag and Cu-Au Nanoclusters Via Copper Hydride Precursors

Rhone P. Brocha Silalahi,[§] Tzu-Hao Chiu,[§] Jhen-Heng Kao,[§] Chun-Yen Wu,[§] Chi-Wei Yin,[†] Yuan Jang Chen,[†]* Yu-Chiao Liu,[¥] Jean-Yves Saillard, [£] Ming-Hsi Chiang,[¥]* and C. W. Liu[§]*

[§]Department of Chemistry, National Dong Hwa University No. 1, Sec. 2, Da Hsueh Rd. Shoufeng, Hualien, Taiwan 974301 (R.O.C.) E-mail:chenwei@mail.ndhu.edu.tw

[†]Department of Chemistry, Fu Jen Catholic University 510 Zhongzheng Rd, Xinzhung Dist. New Taipei City, Taiwan 24205 (R.O.C.)

[¥]Institute of Chemistry, Academica Sinica, Taipei, Taiwan, 11528 (R.O.C.)

[£] Univ Rennes, CNRS, ISCR-UMR 6226, Rennes F-35000, France

Methods: Emission Measurement

Emission spectra and lifetimes in 77 K 2-MeTHF glasses were obtained using calibrated by a Xe lamp for wavelength and an Oriel model 63358 or 63966 Quartz Tungsten Halogen (QTH) lamp for intensity. The emission spectra of complexes were excited by laser 473 nm (MBL-III-473) for complexes **1a-b**, **2a-2c**, and **3**. The emission spectra were collected using a HORIBA JOBIN YVON iHR 550 spectrometer with three gratings (300 l/mm, 600 nm blaze; 300 l/mm, 1 μm blaze; and 600 l/mm, 1 μm blaze) and a HORIBA Symphony InGaAs-1700 (for the NIR) detector head were mounted on the exit port. This system was operated using the SynerJY software. The detector heads were cooled to -90 ^{o}C and the spectrometers were purged with dry N_2. The 77 K emission lifetimes were determined using a LTB Model MNL 103-PD nitrogen laser-pumped a LTB Model DUL 100 Dye laser system for excitation 475 nm for complexes **1a-b**, **2a-2c**, **3** and a Hamamatsu P928 PMT/E717-63 socket assembly mounted on a Jobin-Yvon H-100 spectrometer for detection in the visible region; and a Hamamatsu NIR-PMT Modul H10330A-75 for collection in the NIR region. Both detector systems for detection in the visible and NIR regions were output digitized using a LeCroy WaveRunner 6030A.

Procedures of emission quantum yields ($\Phi_{(em)}$) of complexes in butyronitrile and alcohol solution were obtained by using $[Ru(bpy)_3]^{2+}$ as references.[1-4] $[Ru(bpy)_3]^{2+}$ at RT ethanol/methanol (alcohol) as a references for the determination emission quantum yields. The quantum yields reported for $[Ru(bpy)_3]^{2+}$ is $\Phi_{(em)r} \approx 0.089$ [5] in alcohol (degas) used as a reference to determine the relative quantum yields for the complexes studied. Equation S1 was used to calculate the relative quantum yield of the target complex ($\Phi_{(em)tc}$)[6, 7]

$$\frac{\Phi_{(em)tc}}{\Phi_{(em)r}} = \frac{\eta_{tc}^{\,2} I_{tc}}{\eta_r^{\,2} I_r} \times \frac{1-10^{-A_r}}{1-10^{-A_{tc}}} \approx \frac{I_{tc} A_r}{I_r A_{tc}} \qquad \text{(S1)}$$

where I_{tc} and I_r are the integrated areas under the emission spectra for the target complex (tc) and the reference (r), respectively, A_{tc} and A_r are the absorbance of interest, respectively, η is refractive index of the solvent, $\eta_r = 1.35$ (alcohol)[8] and $\eta_{tc} = 1.41$ (2-MeTHF)[9]. The sample path length for the absorbance in eq S1, is not well defined for these cells, but the effective pathlengths did not vary much since the cell geometry and position were the same for both the sample and reference solutions.[1-4] Solute concentrations (10^{-5}~10^{-6} M) had to be taken

into account, in order to achieve absorbances 1 in 1 cm; but in the 2 mm id cylindrical cells this amounts to an absorbance of considerably less than 0.2 in the sample solutions and relatively higher solute concentrations were used for weakly absorbing and/or very weakly emitting substrates. Solutions that showed signs of inhomogeneity (light scattering, broadened and anomalous spectra and/or multicomponent and irreproducible decay behavior) were discarded.

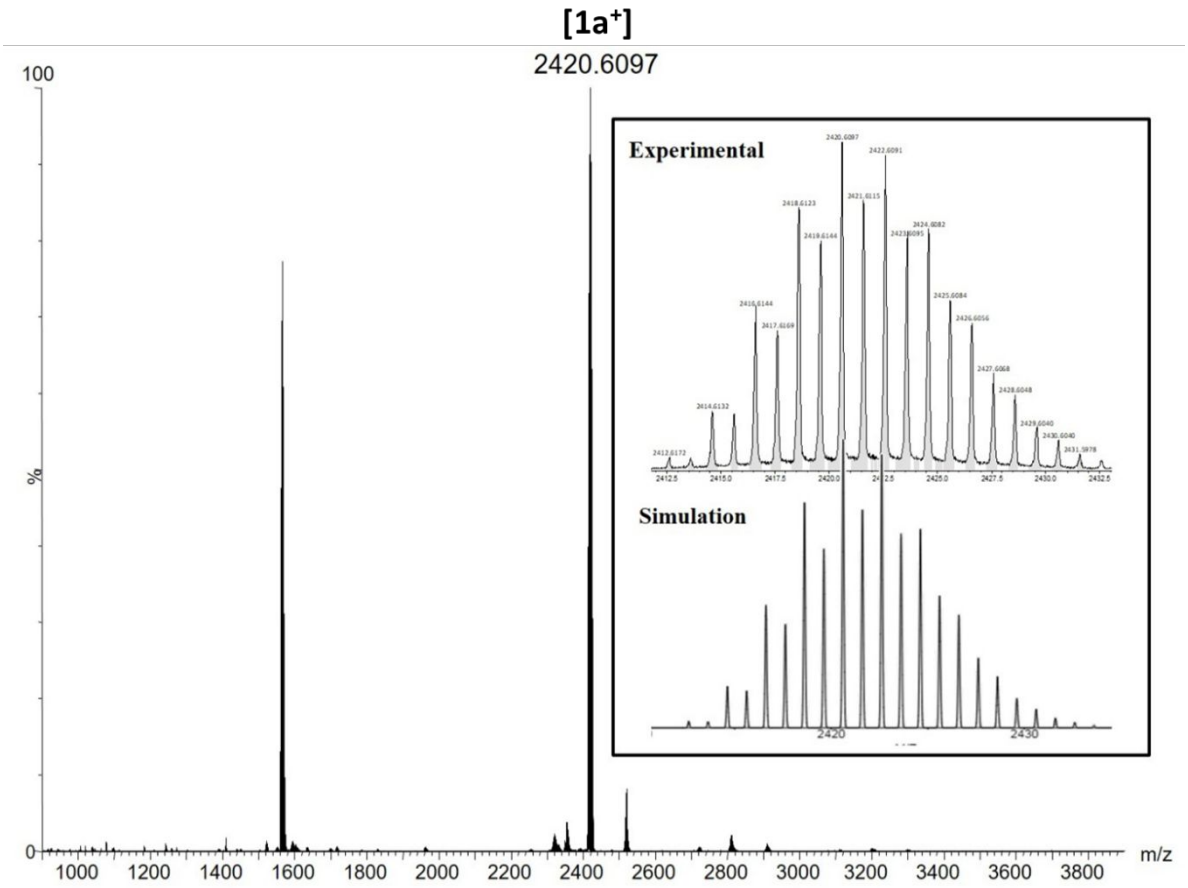

Figure S1. The ESI-MS spectra of cluster **1a**$^{+}$ in positive mode. Insets show both experimental and simulated isotope patterns.

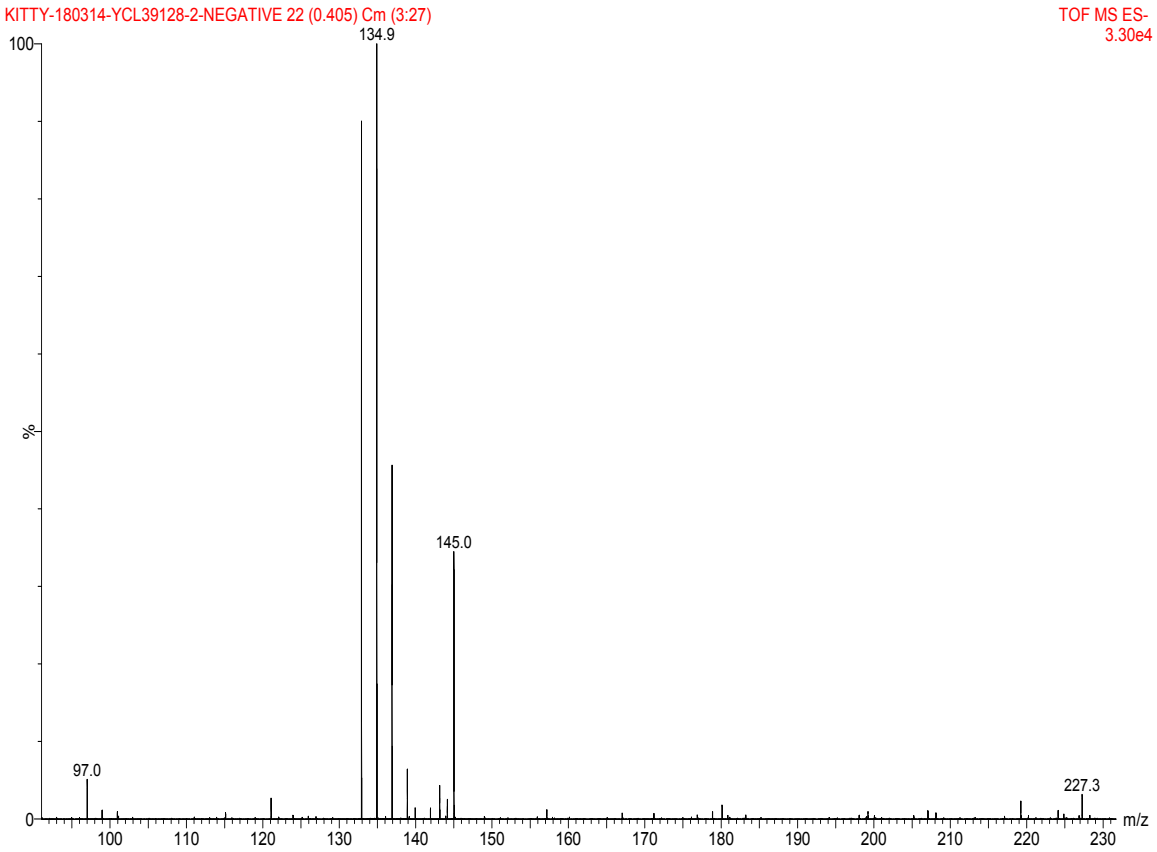

Figure S2. Negative mode ESI-MS spectrum of cluster **1a**.

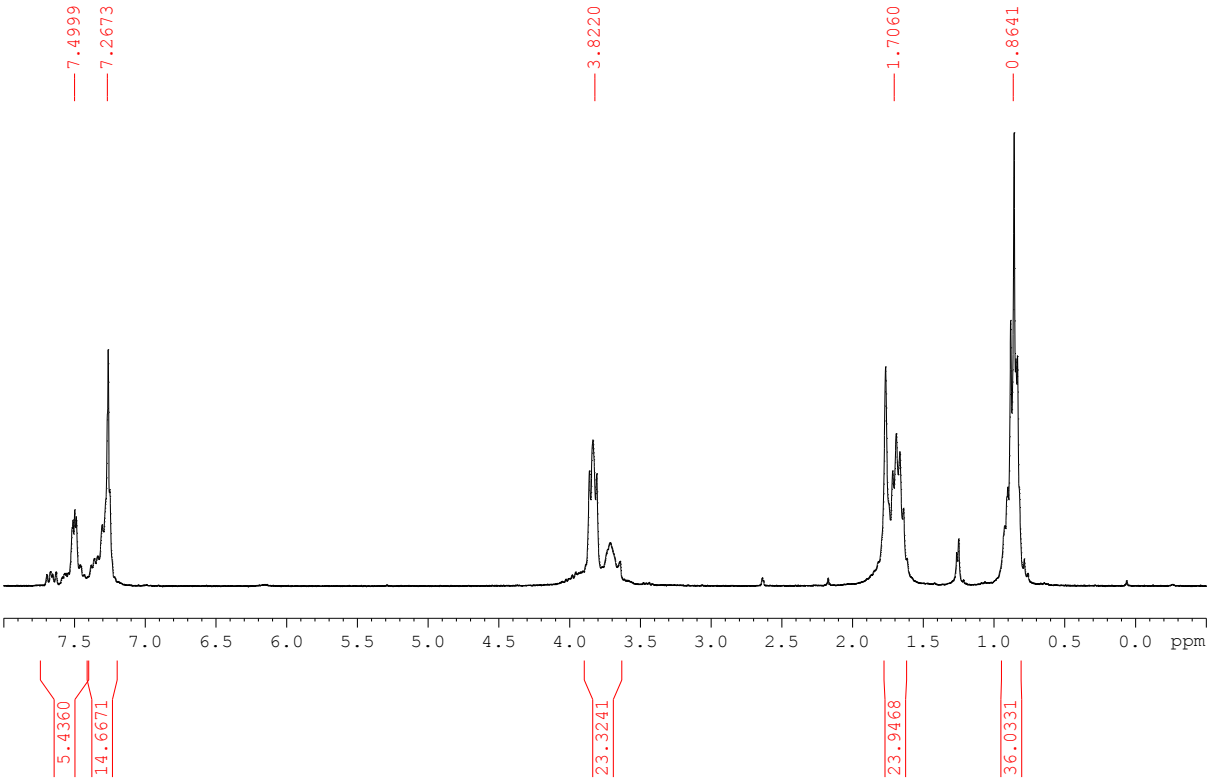

Figure S3. ^{1}H NMR spectrum of cluster **1a** in d-chloroform.

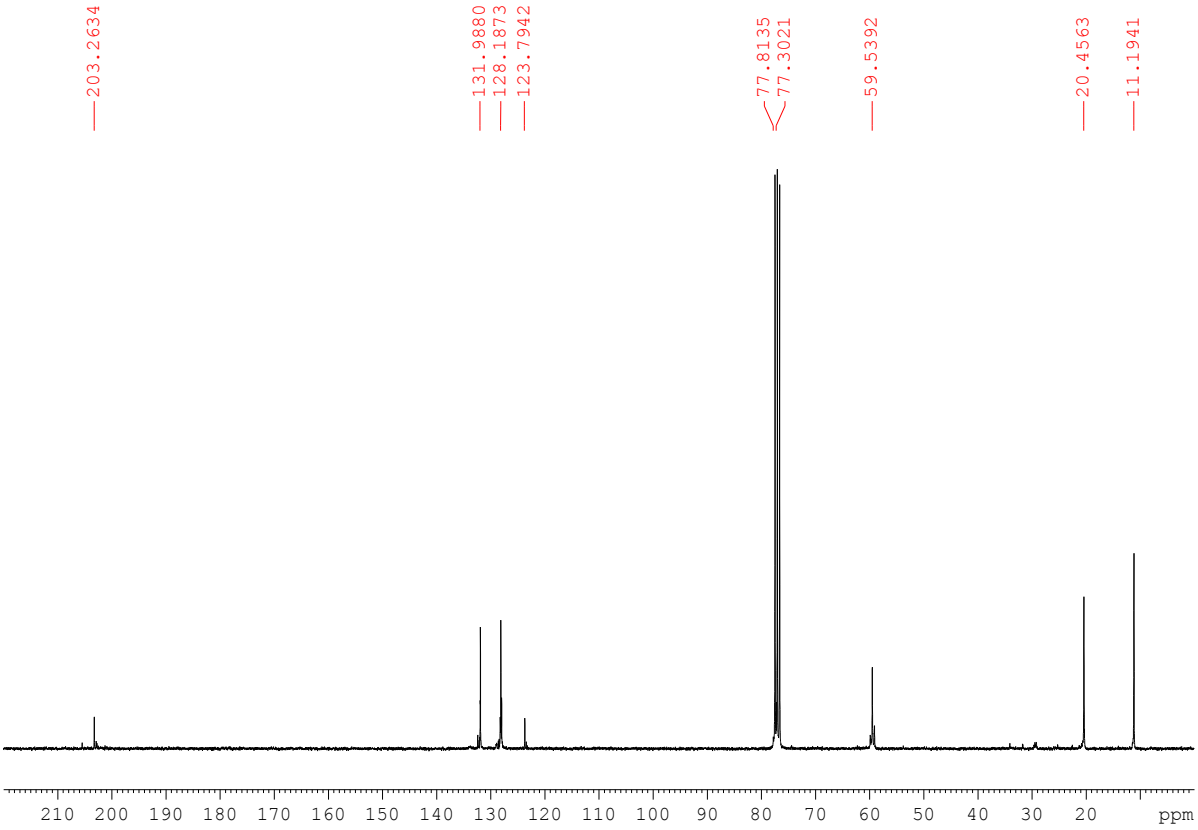

Figure S4. ^{13}C NMR spectrum of cluster **1a** in *d*-chloroform.

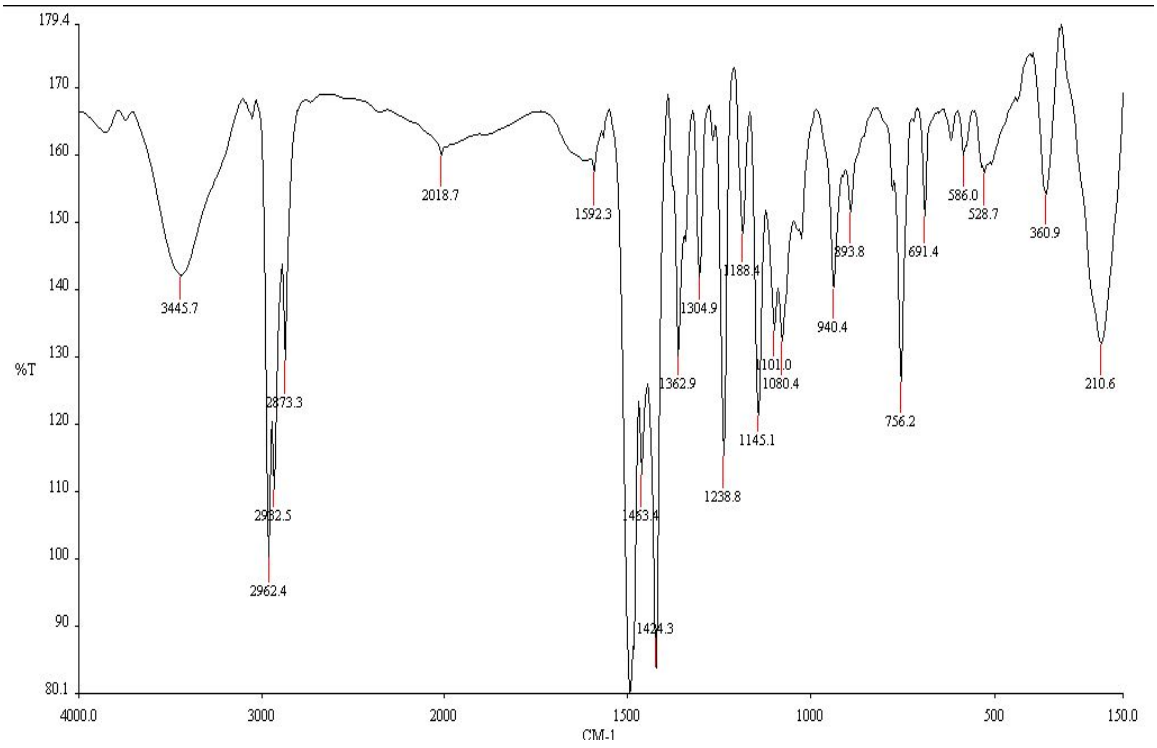

Figure S5. IR spectrum of cluster **1a**.

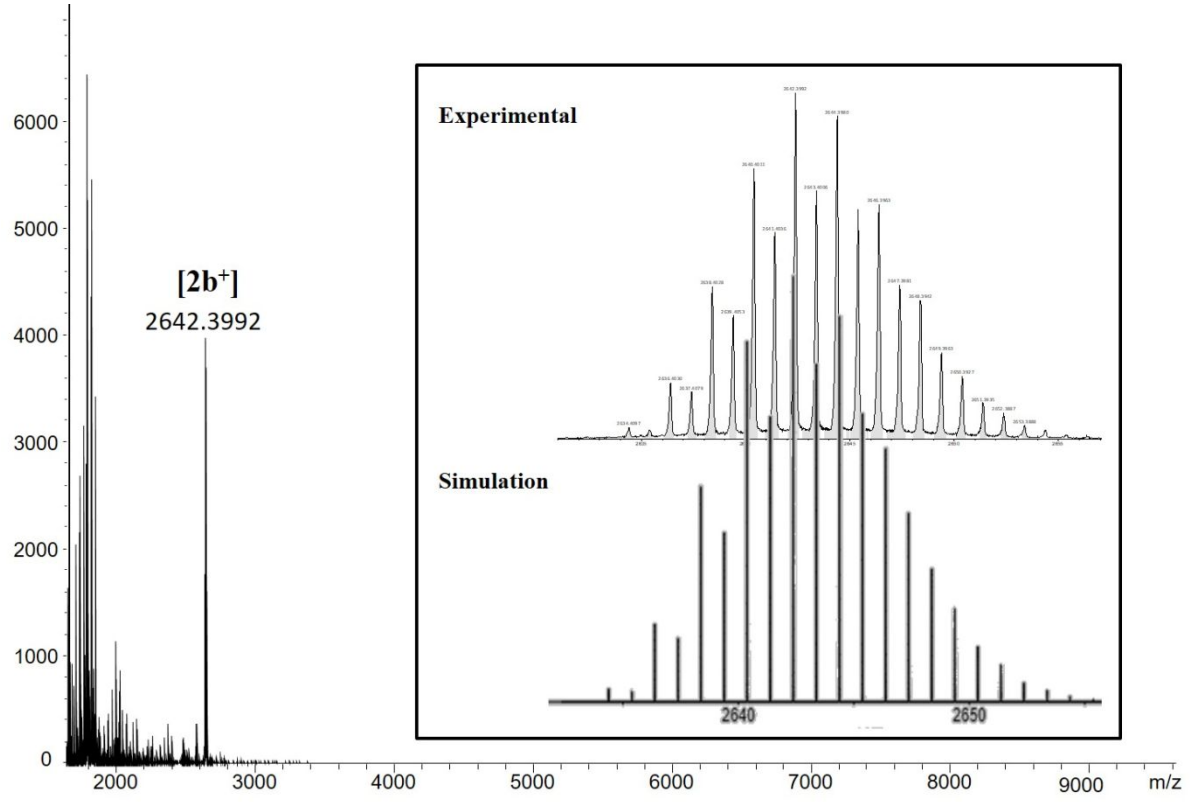

Figure S6. Positive mode ESI-Ms spectra of cluster **2b**$^{+}$. The top and bottom insets show the experimental and simulation ones, respectively.

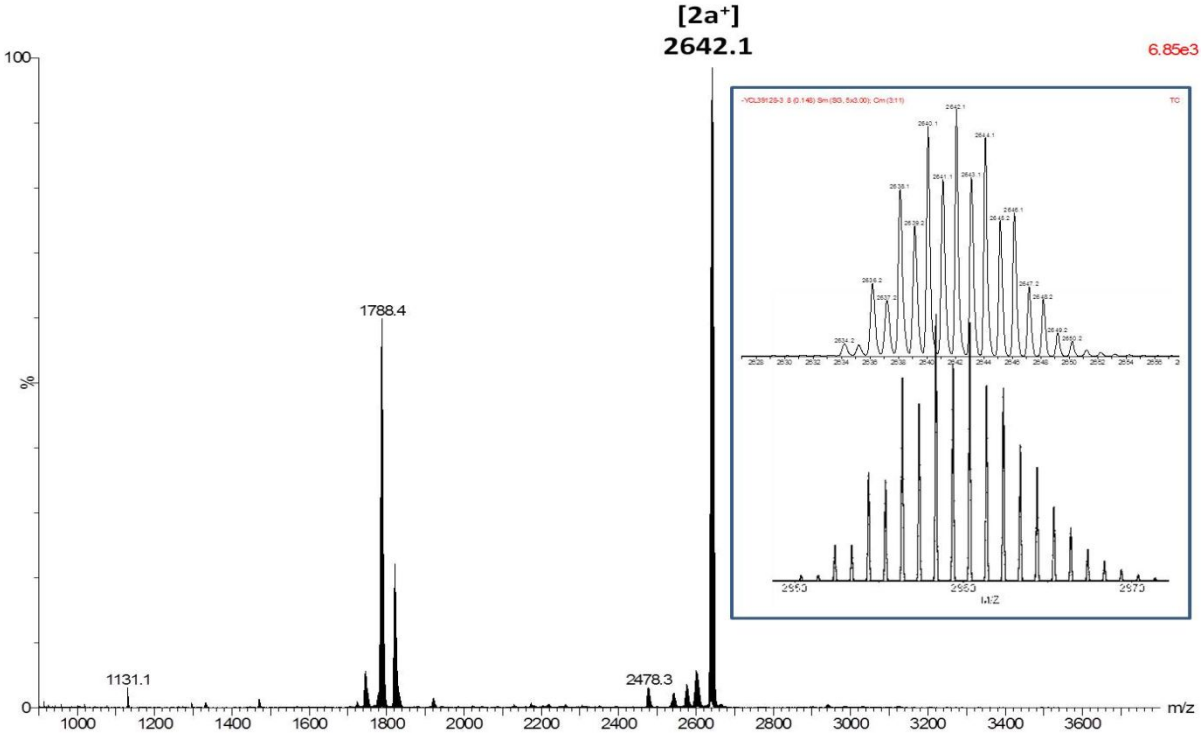

Figure S7. Positive mode ESI-Ms spectra of cluster **2a**$^{+}$. The top and bottom insets show the experimental and simulation ones, respectively.

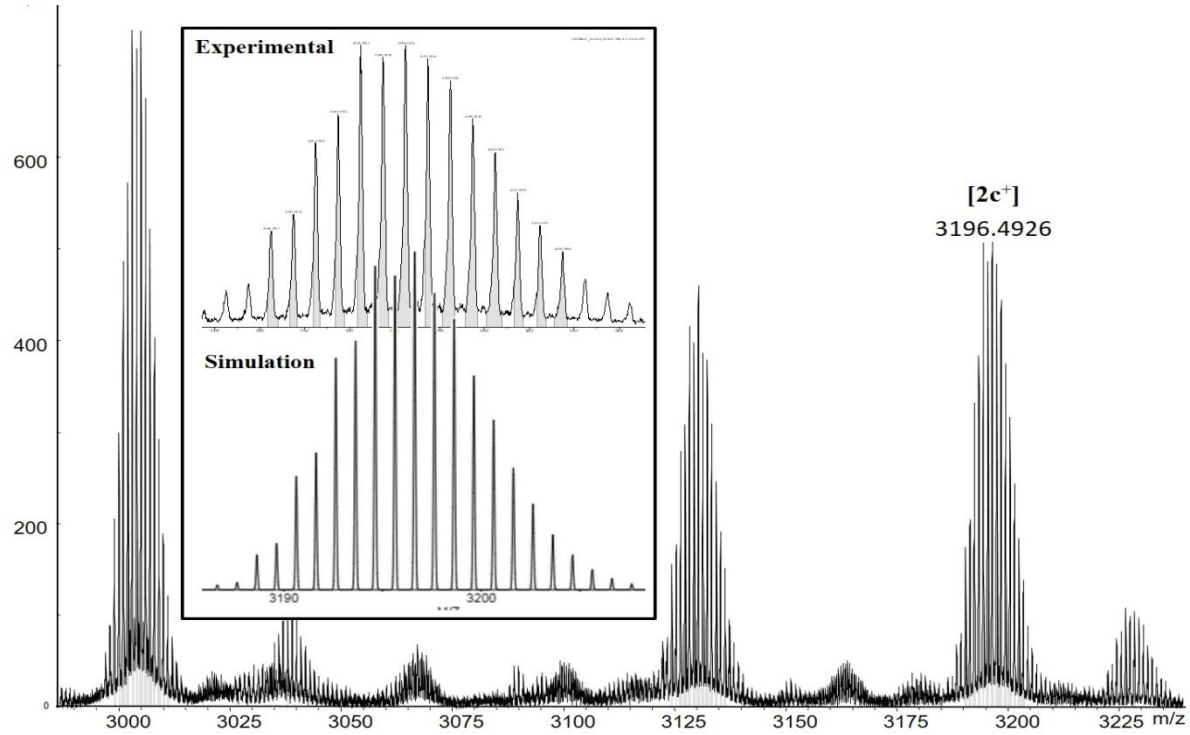

Figure S8. Positive mode ESI-Ms spectra of cluster **2c**$^{+}$. The top and bottom insets show the experimental and simulation ones, respectively.

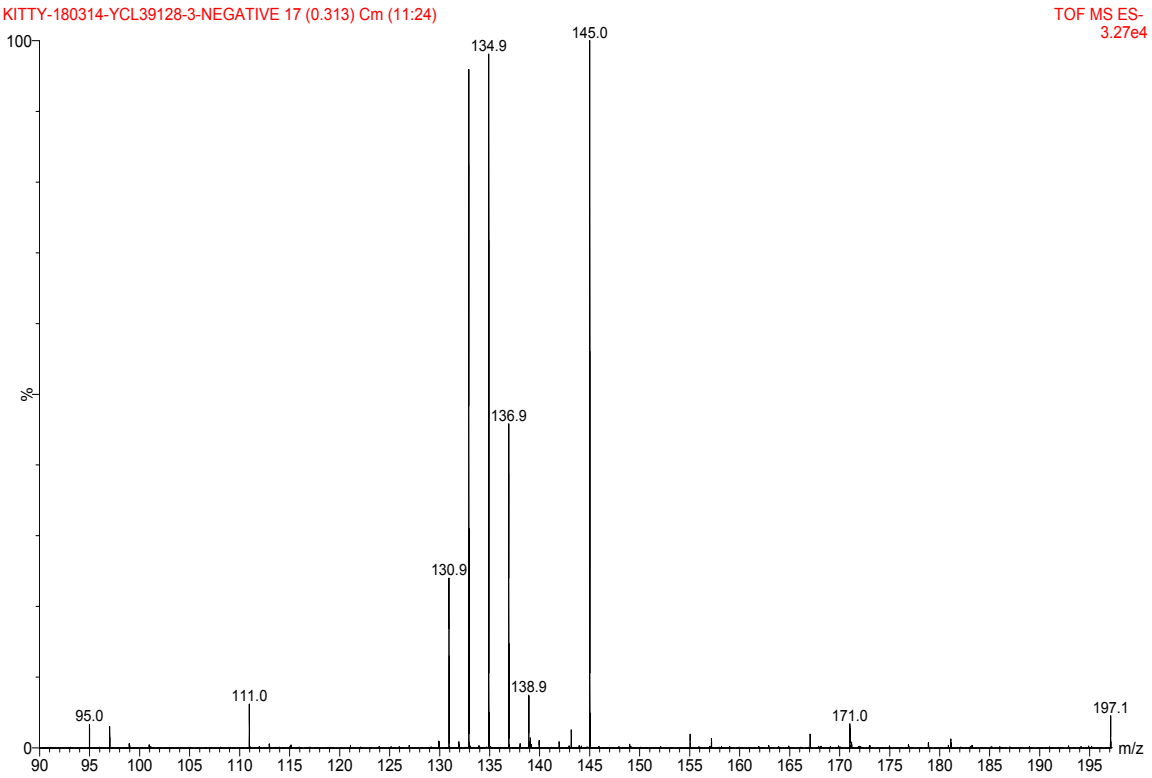

Figure S9. Negative mode ESI-Ms spectrum of cluster **2a**.

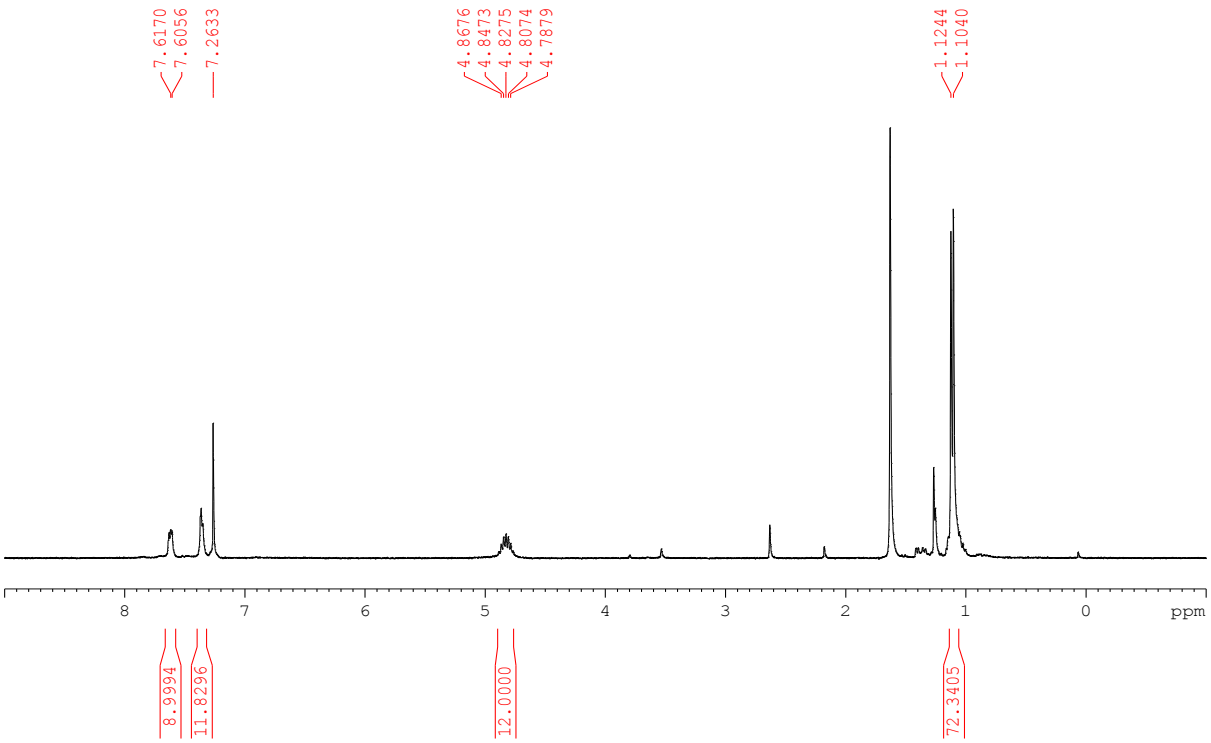

Figure S10. [1]H NMR spectrum of cluster **2a** in *d*-chloroform.

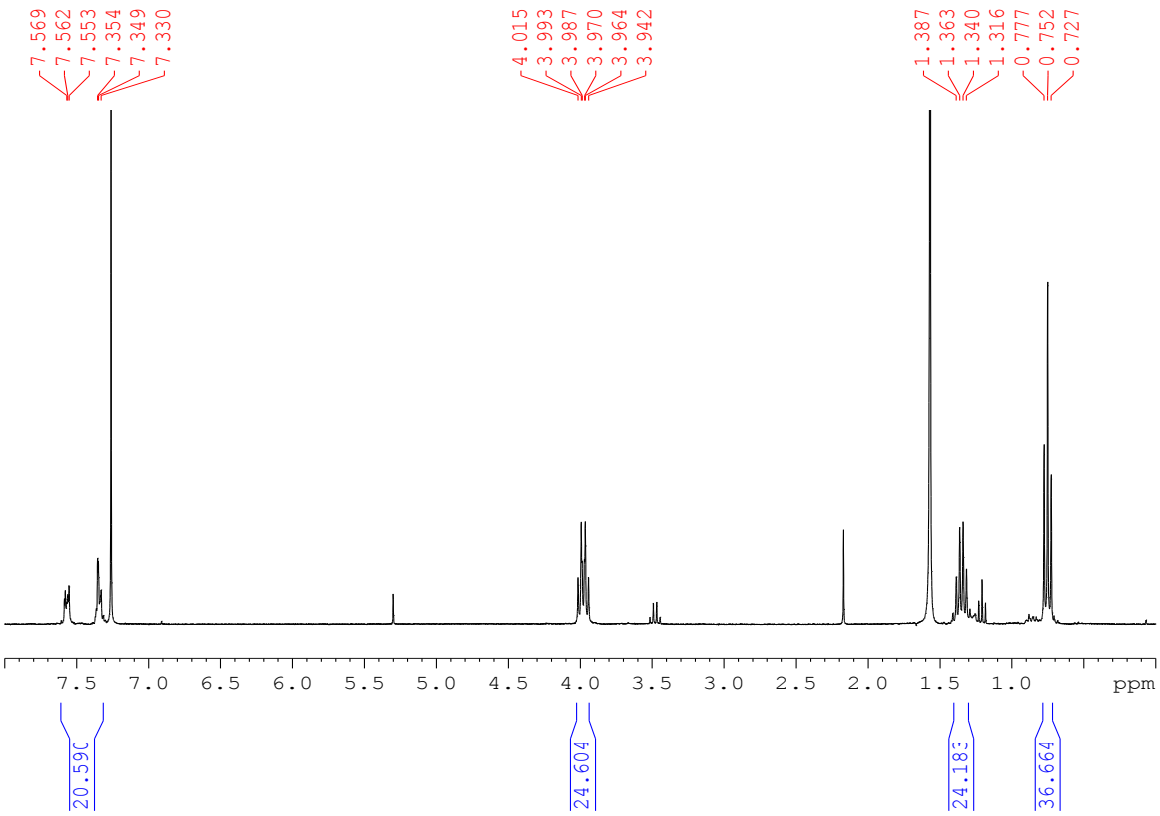

Figure S11. [1]H NMR spectrum of cluster **2b** in *d*-chlroform.

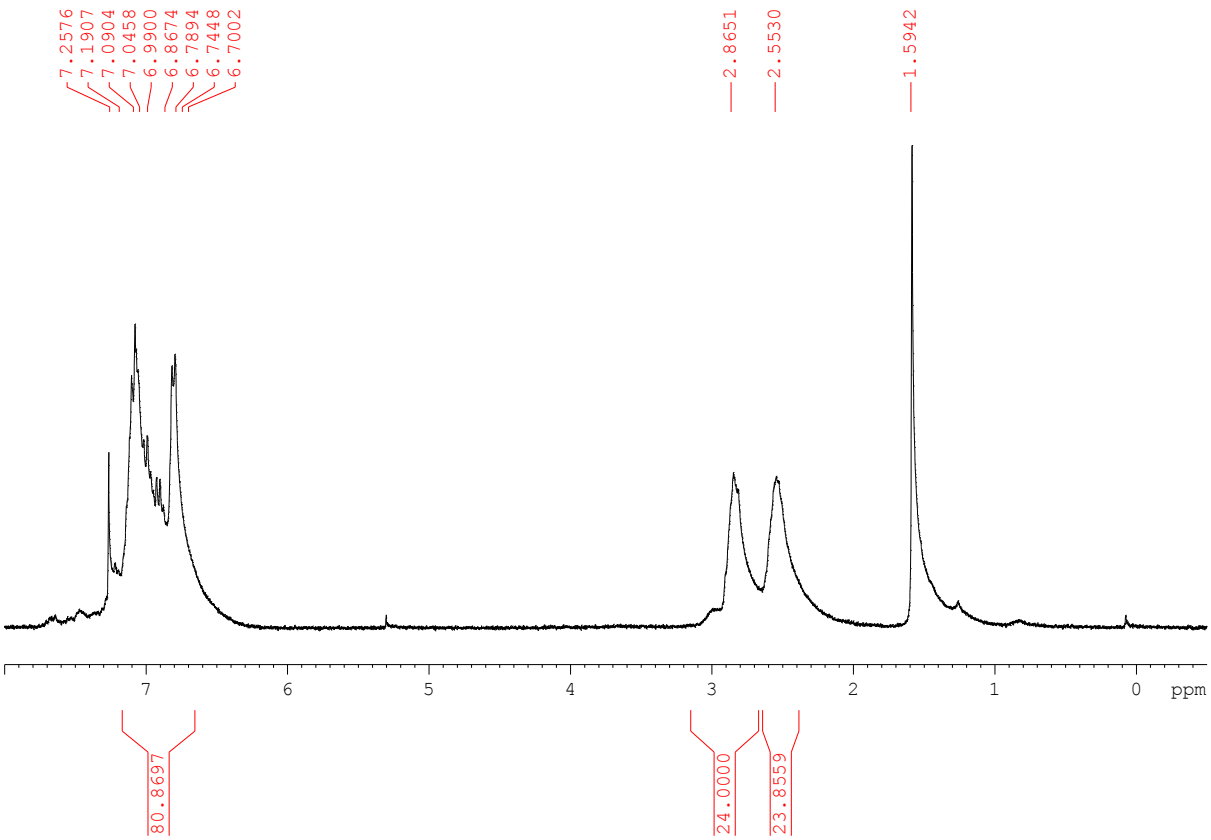

Figure S12. [1]H NMR spectrum of cluster **2c** in *d*-chloroform.

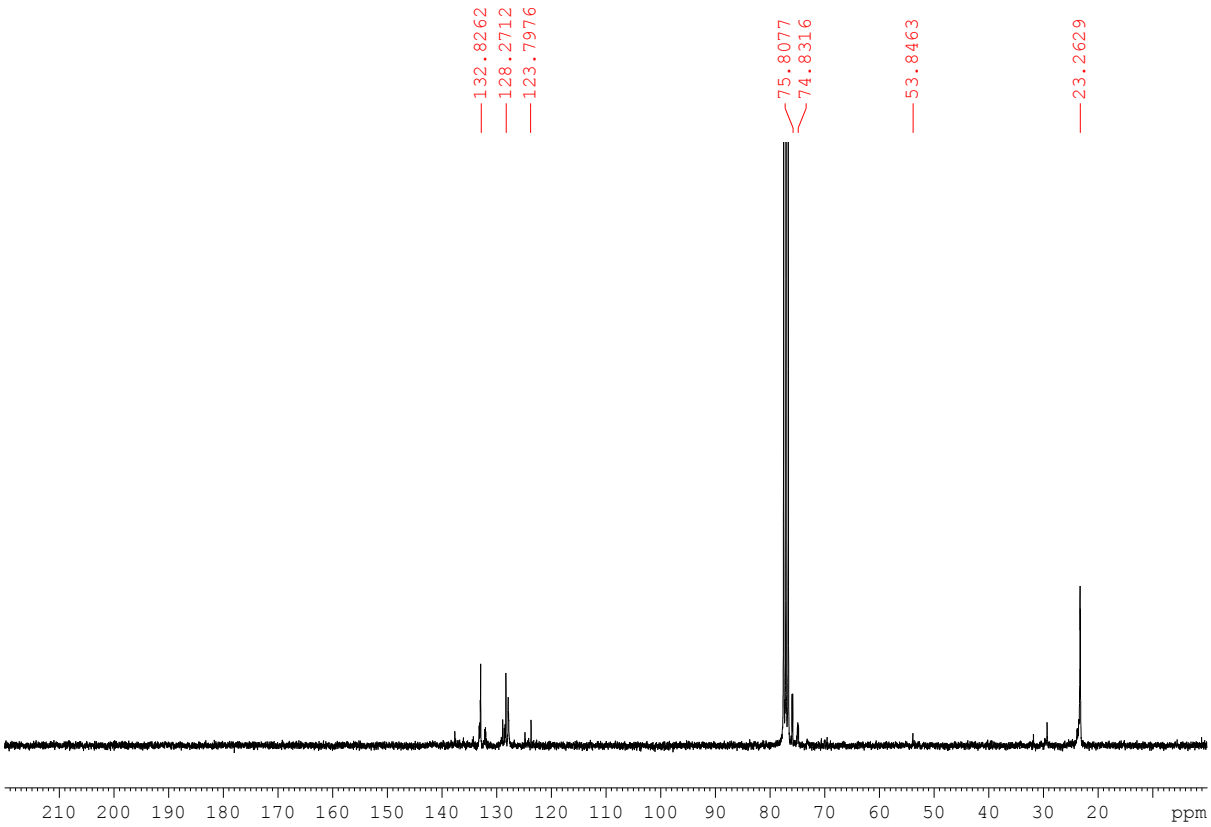

Figure S13. [13]C NMR spectrum of cluster **2a** in *d*-chloroform.

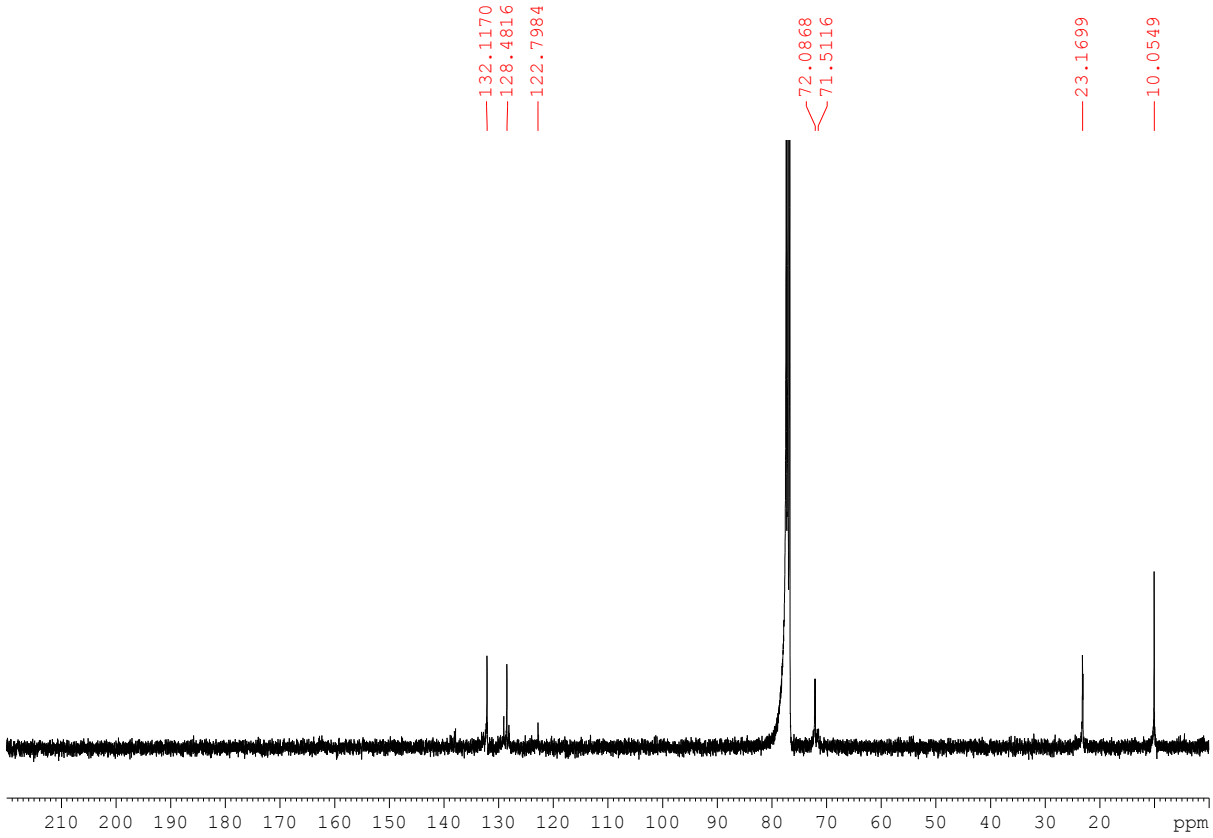

Figure S14. ^{13}C NMR spectrum of cluster **2b** in *d*-chloroform.

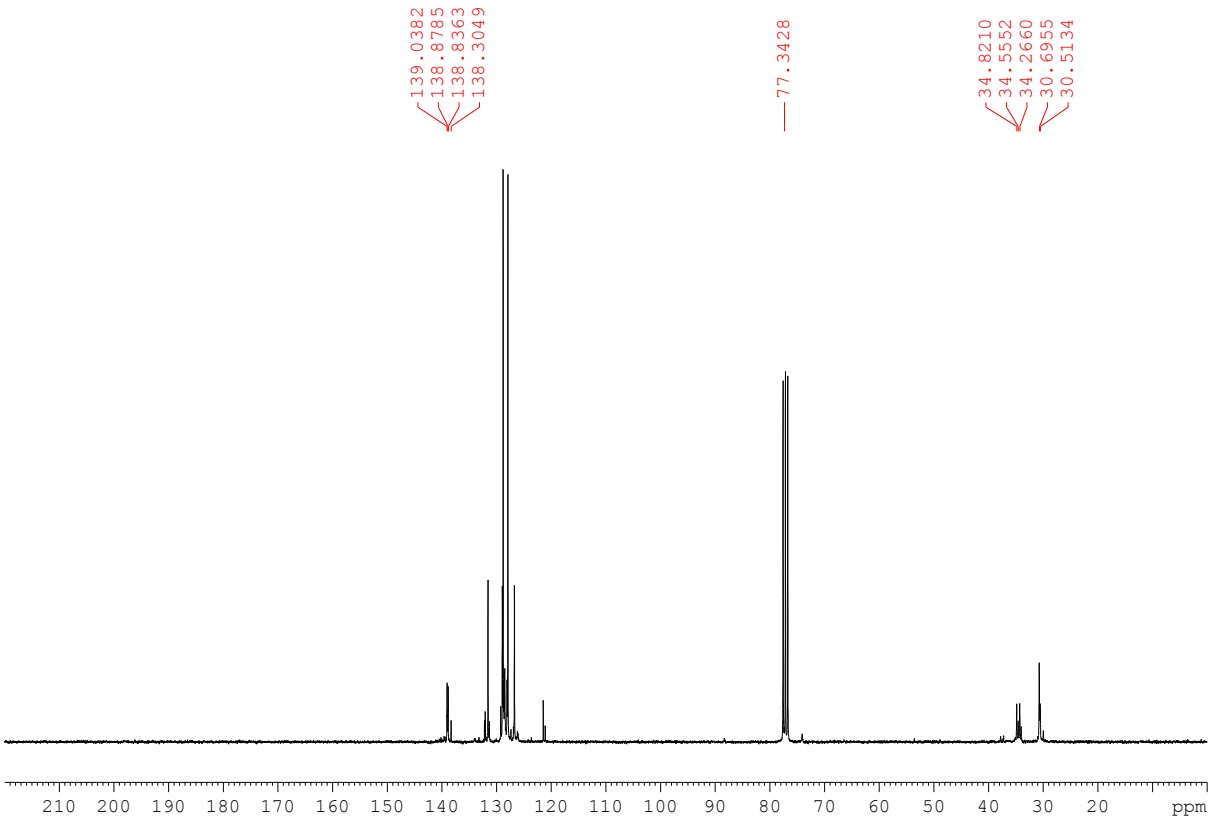

Figure S15. ^{13}C NMR spectrum of cluster **2c** in *d*-chloroform.

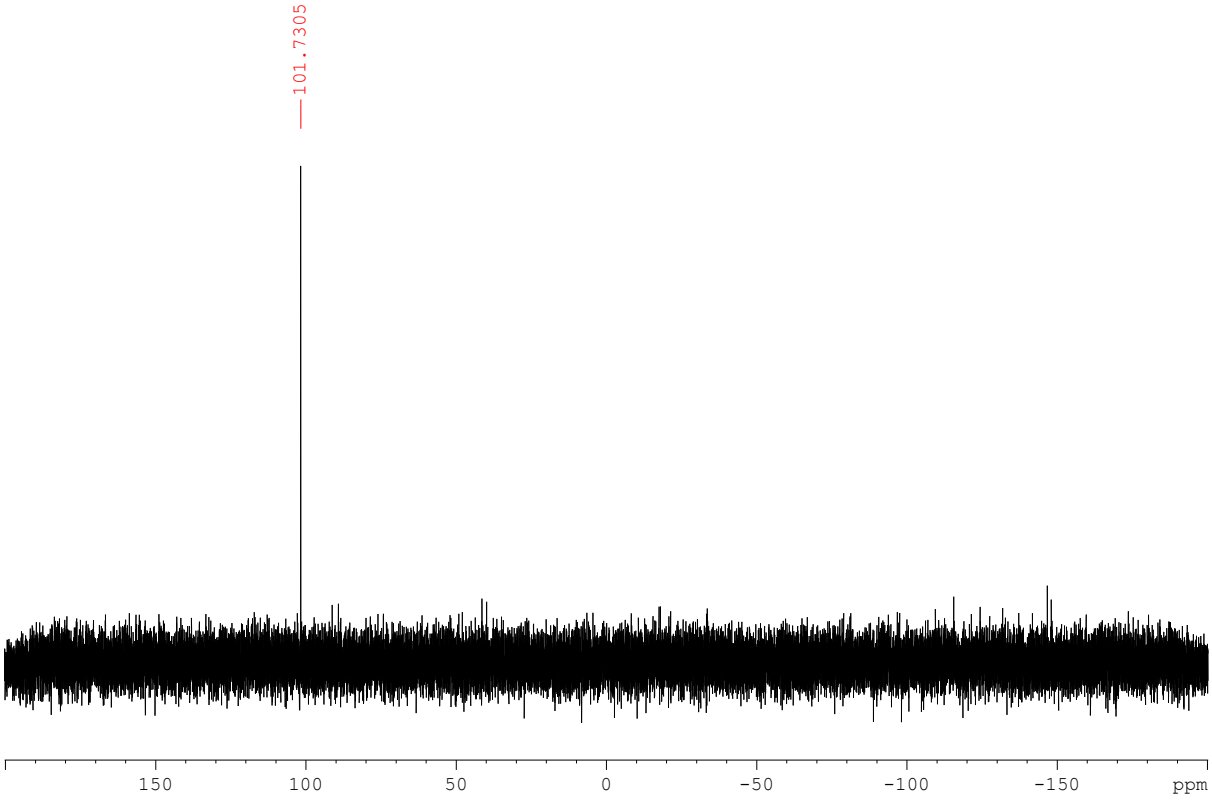

Figure S16. $^{31}P\{^{1}H\}$ NMR spectrum of cluster **2a** in *d*-chloroform.

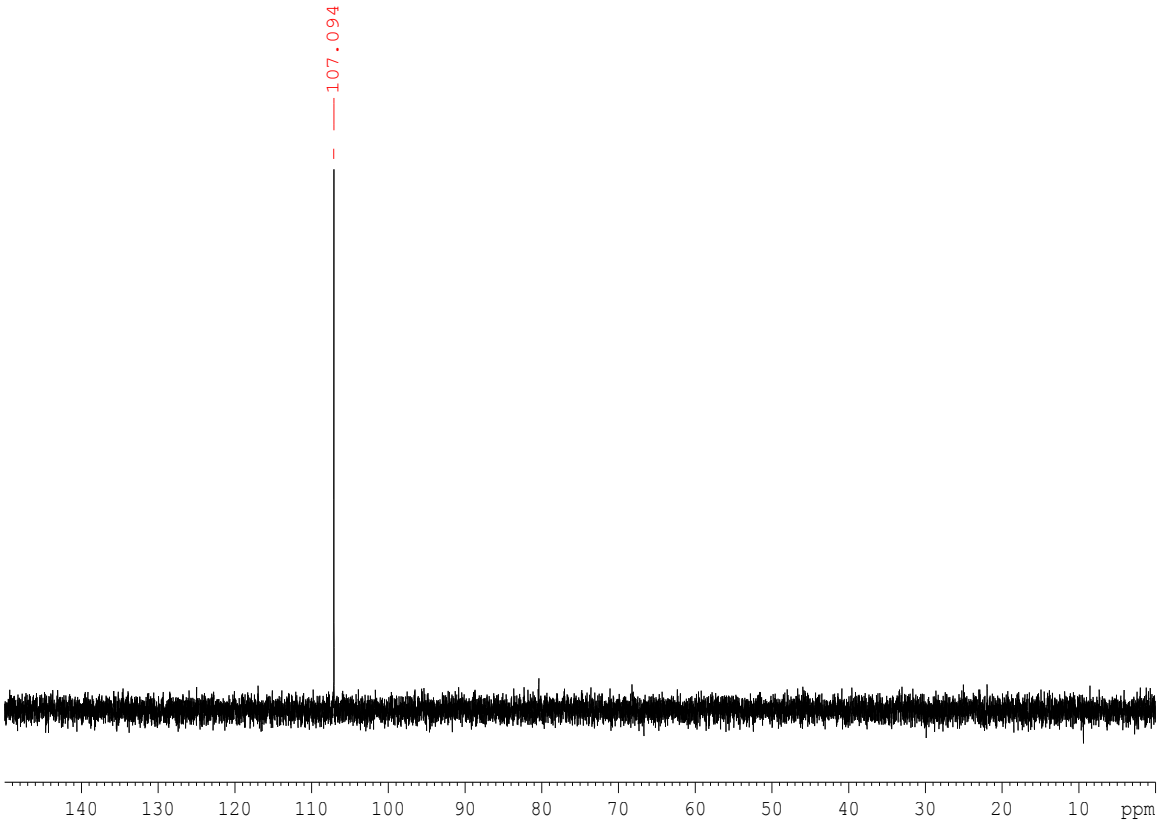

Figure S17. $^{31}P\{^{1}H\}$ NMR spectrum of cluster **2b** in *d*-chloroform.

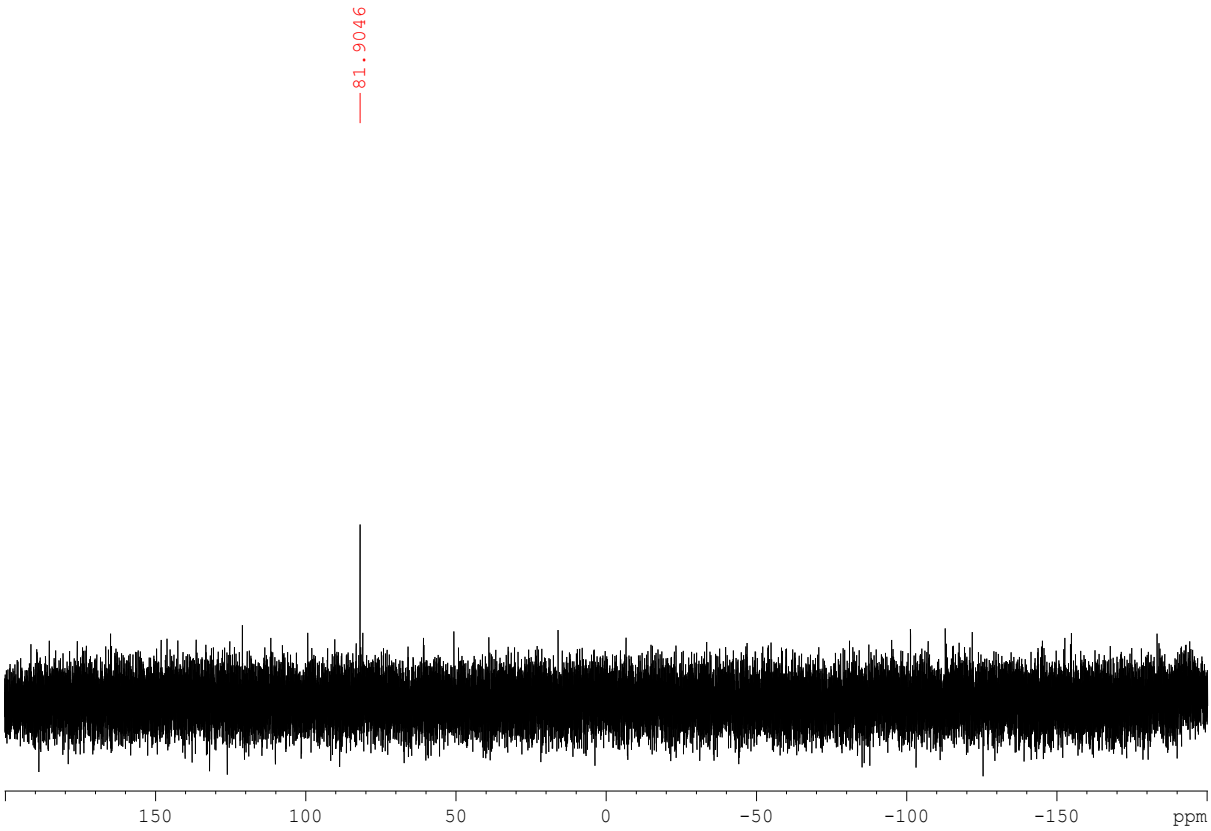

Figure S18. $^{31}P\{^{1}H\}$ NMR spectrum of cluster **2c** in *d*-chloroform

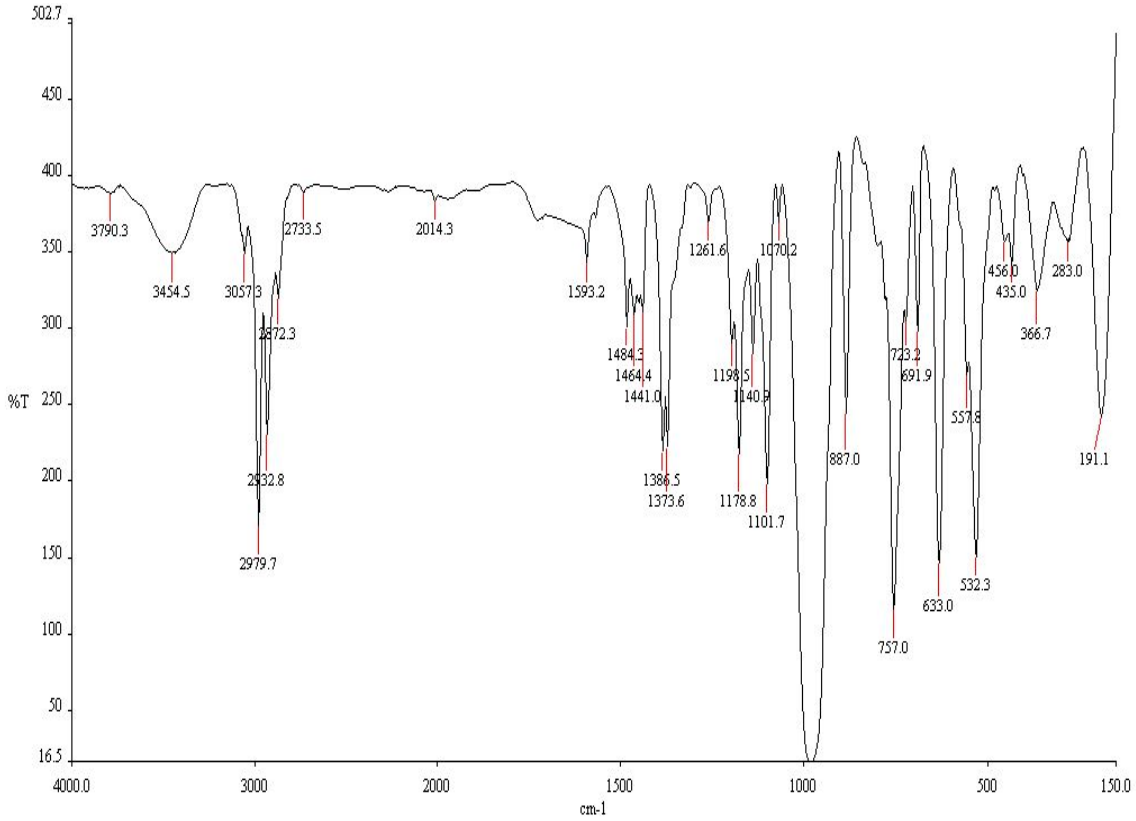

Figure S19. IR spectrum of cluster **2a**.

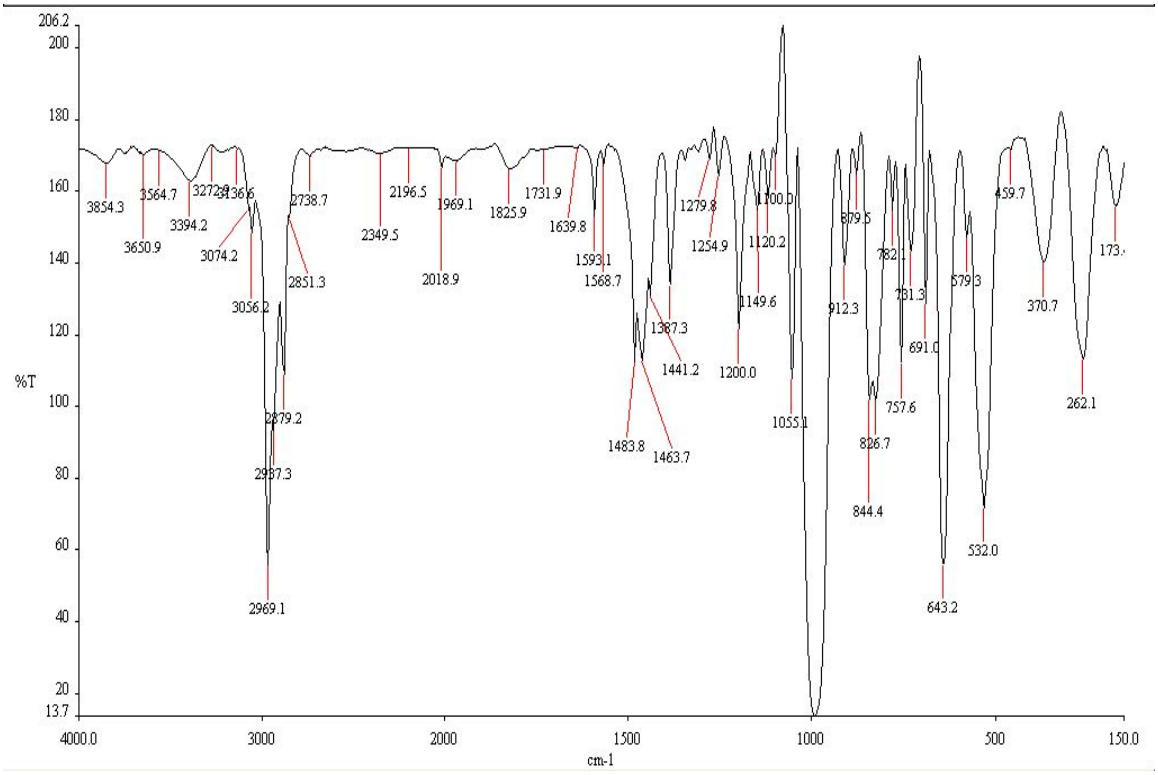

Figure S20. IR spectrum of cluster **2b**.

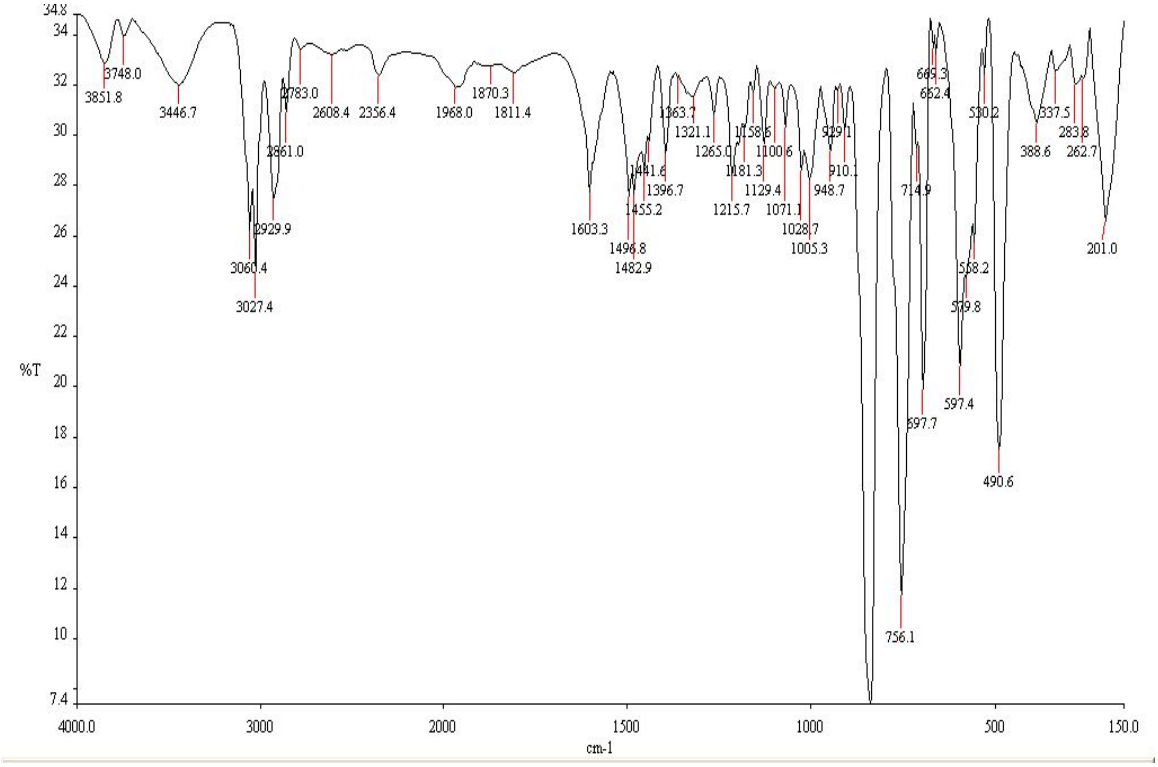

Figure S21. IR spectrum of cluster **2c**.

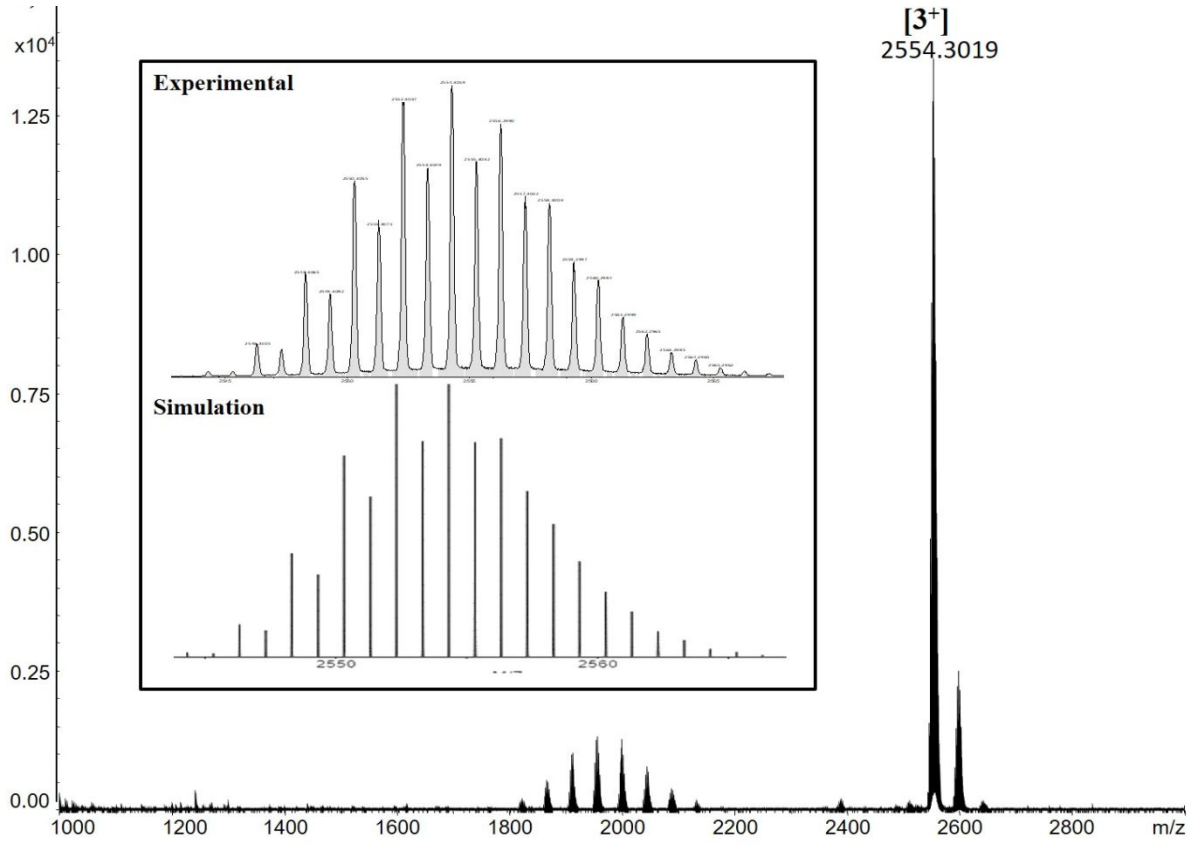

Figure S22. Positive mode ESI-Ms spectra of cluster $\mathbf{3}^{+}$. The top and bottom insets show the experimental and simulation ones, respectively.

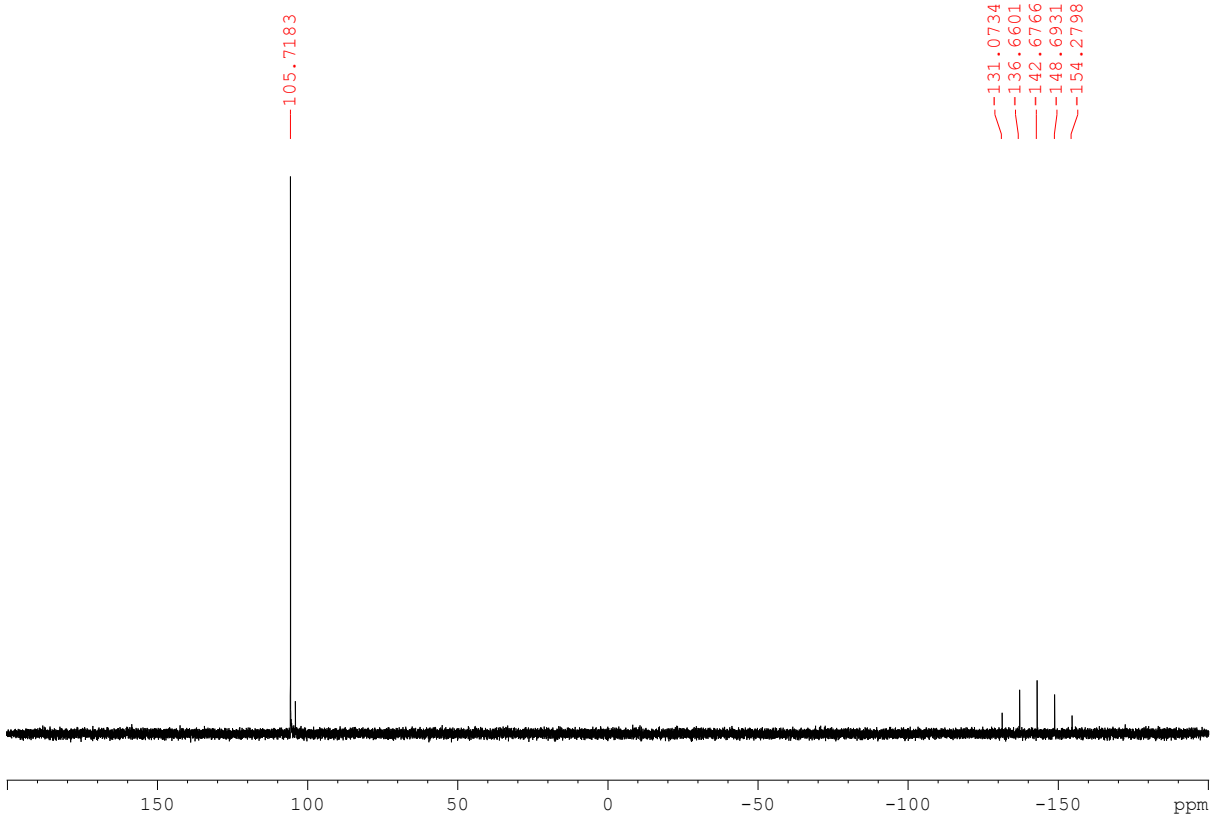

Figure S23. $^{31}P\{^{1}H\}$ NMR spectrum of cluster **3** in d_6-acetone.

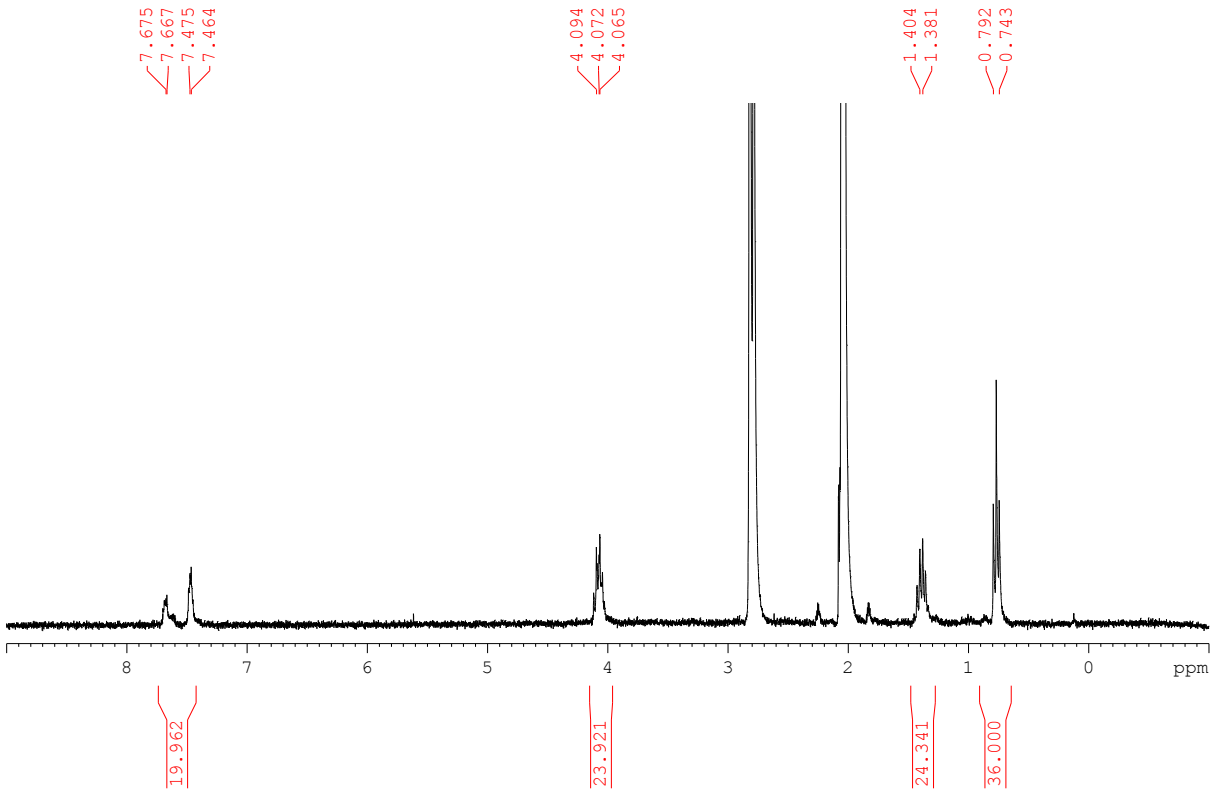

Figure S24. ^{1}H NMR spectrum of cluster **3** in d_6-acetone.

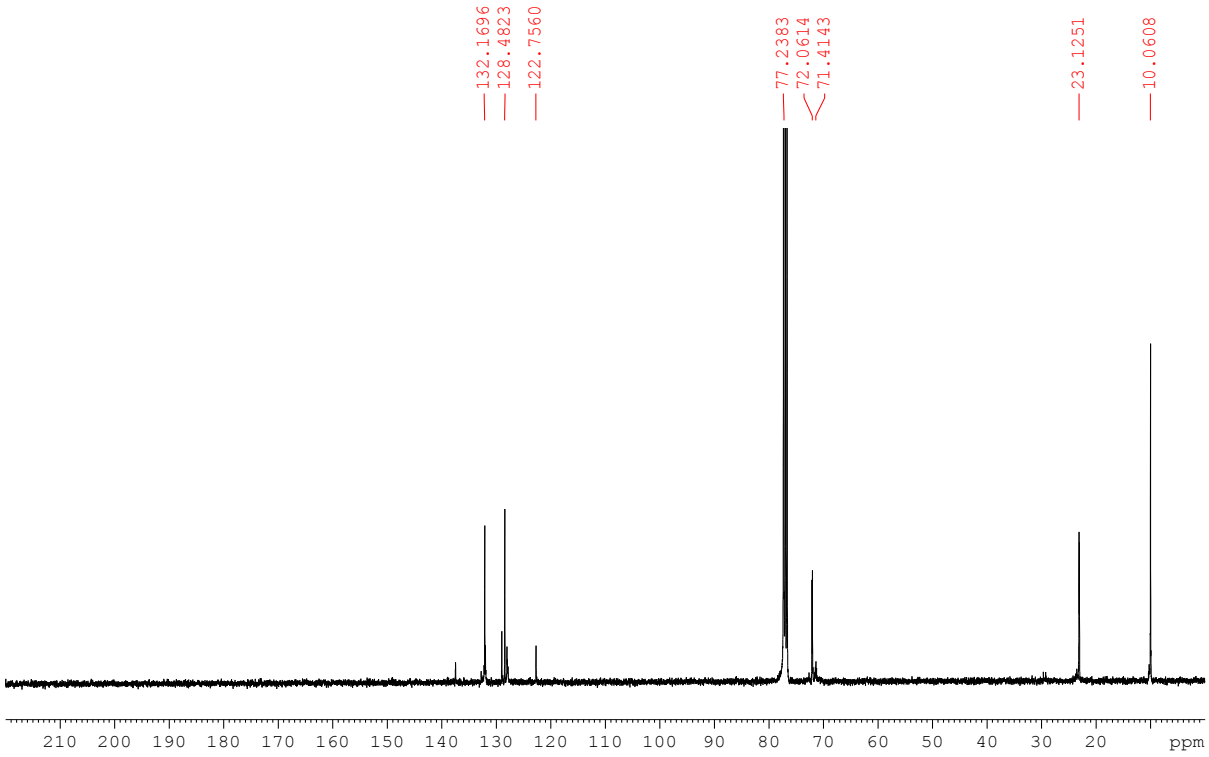

Figure S25. ^{13}C NMR spectrum of cluster **3** in *d*-chloroform.

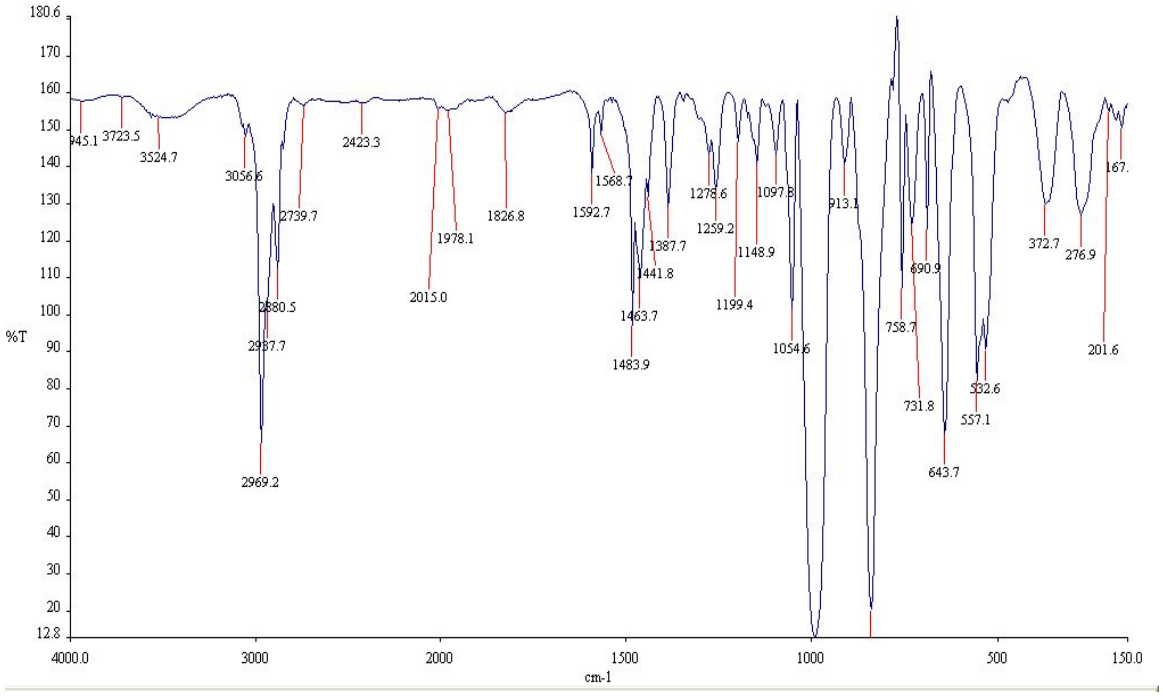

Figure S26. IR spectrum of cluster **3**.

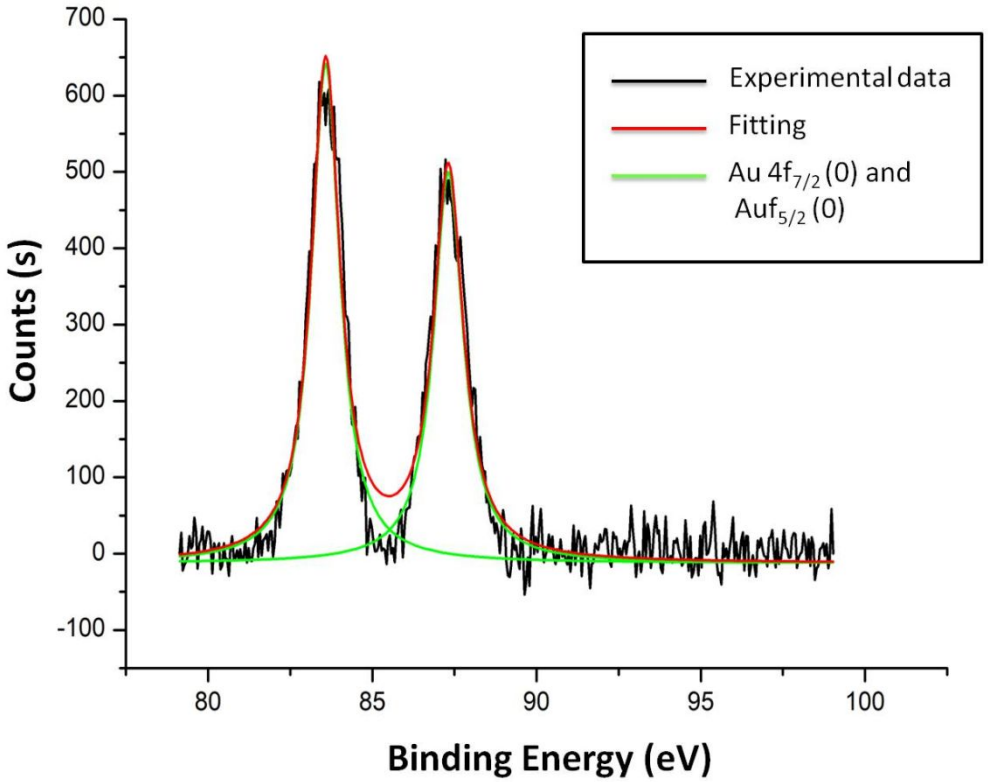

Figure S27. The Au 4f spectrum in X-ray photoelectron spectroscopy (XPS) of cluster **1a**.

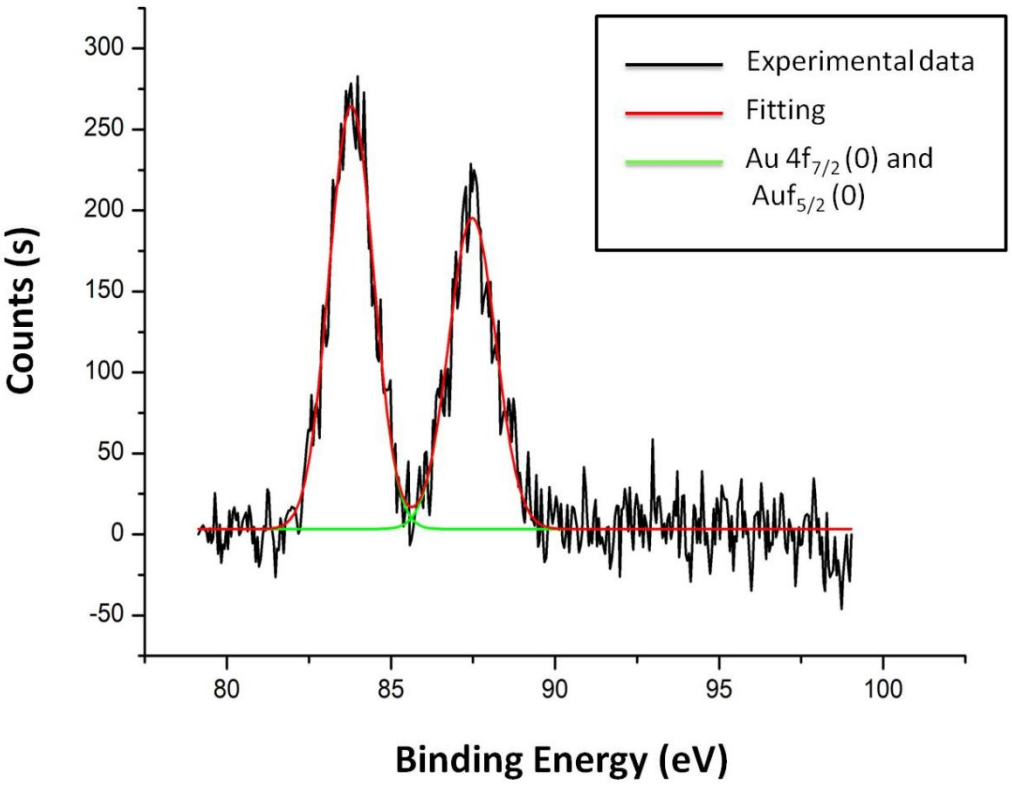

Figure S28. The Au 4f spectrum in X-ray photoelectron spectroscopy (XPS) of cluster **2a**.

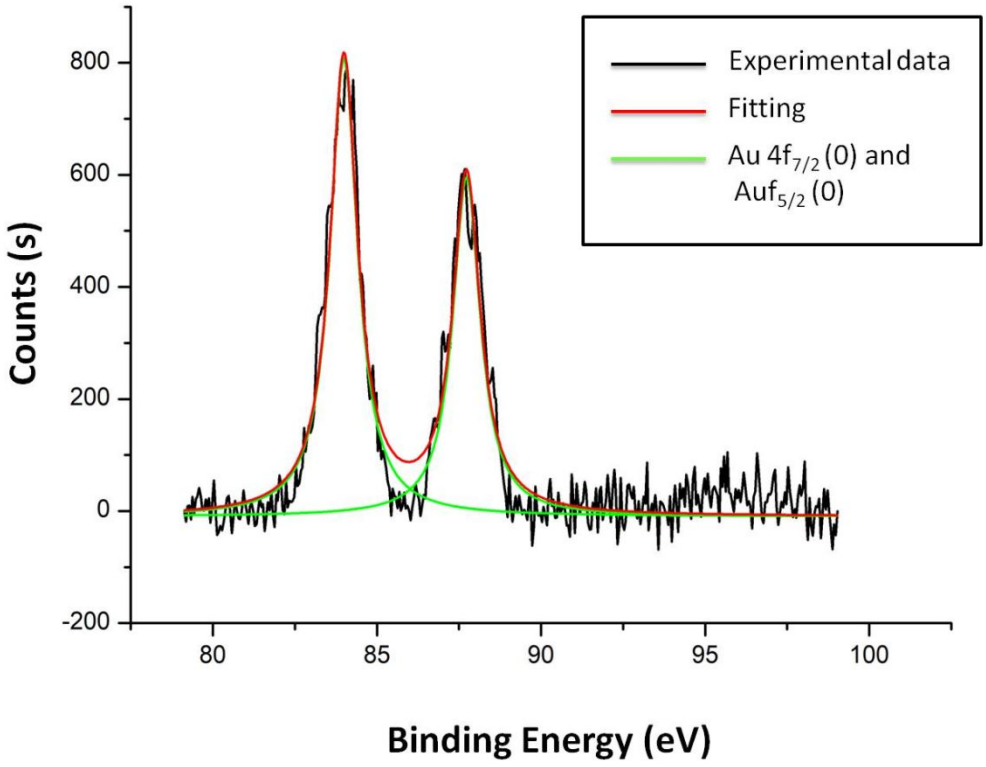

Figure S29. The Au 4f spectrum in X-ray photoelectron spectroscopy (XPS) of cluster **2b**.

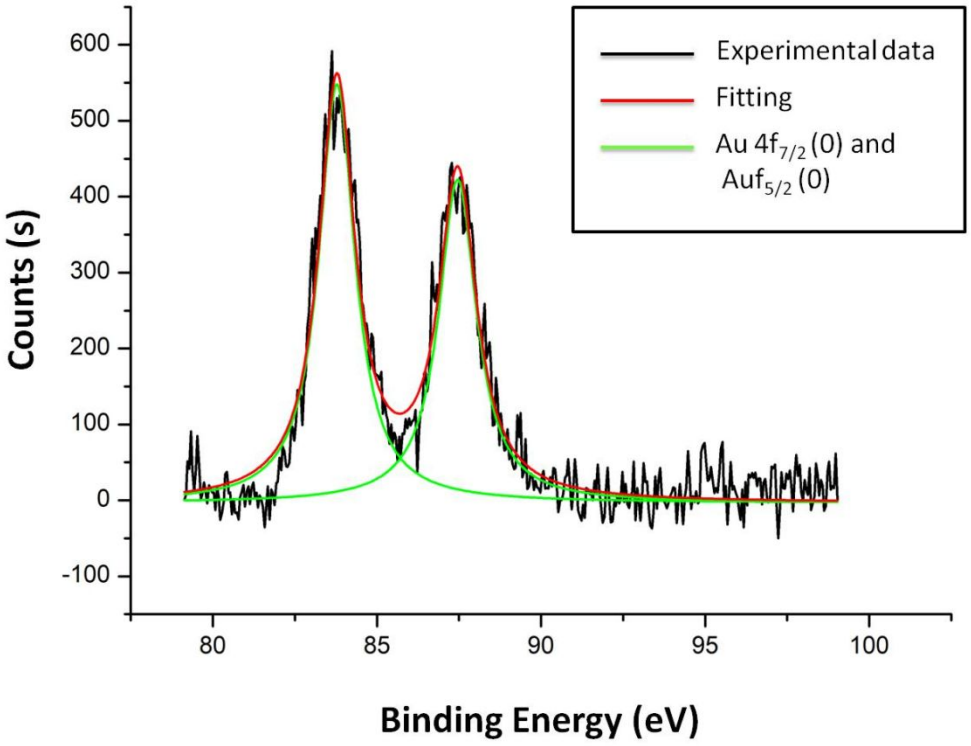

Figure S30. The Au 4f spectrum in X-ray photoelectron spectroscopy (XPS) of cluster **2c**.

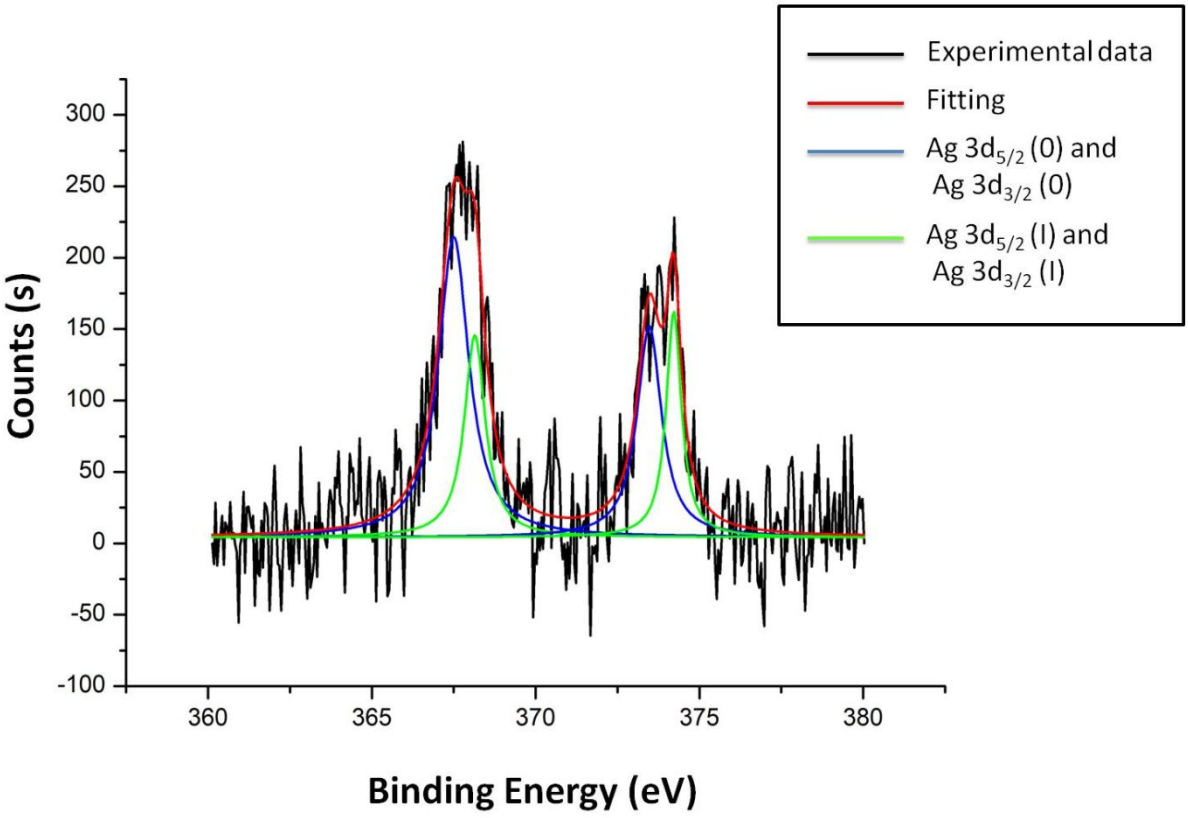

Figure S31. The Ag 3d spectrum in X-ray photoelectron spectroscopy (XPS) of cluster **3**.

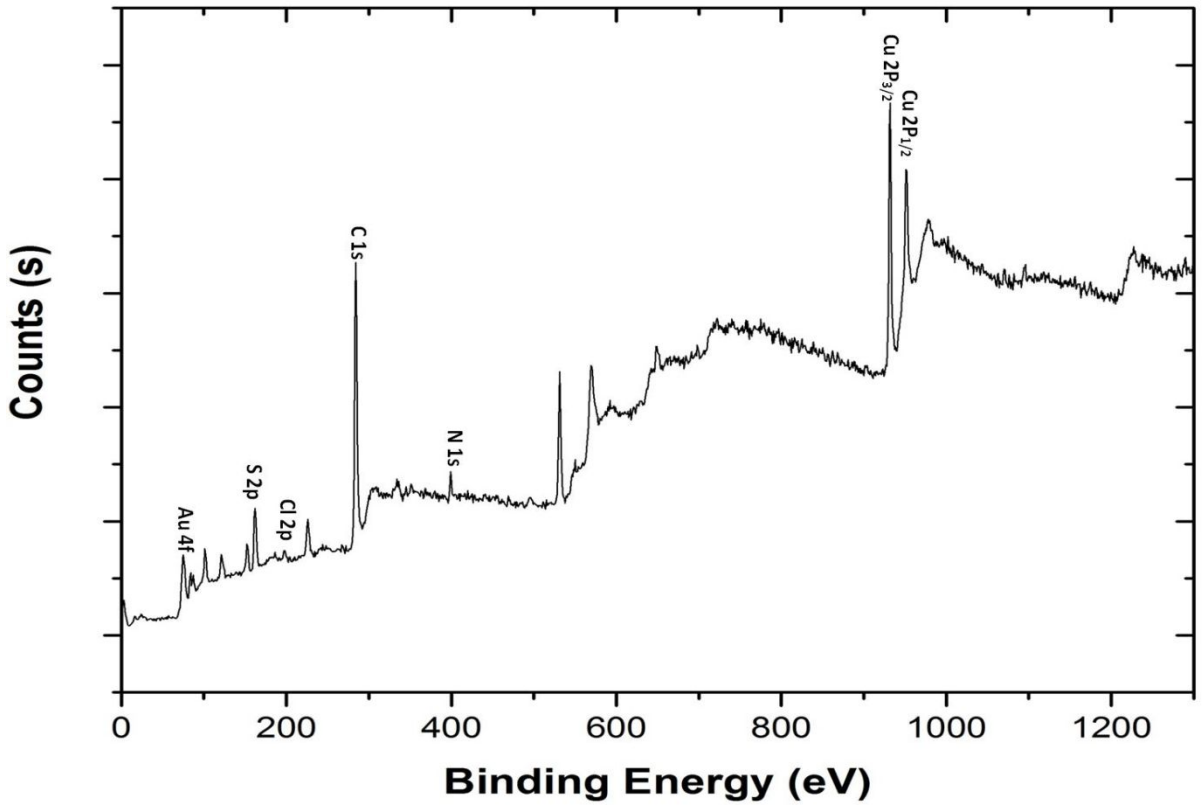

Figure S32. XPS survey spectrum of cluster **1a**. It identifies the presence of copper, sulfur, carbon, nitrogen, fluorine and oxygen.

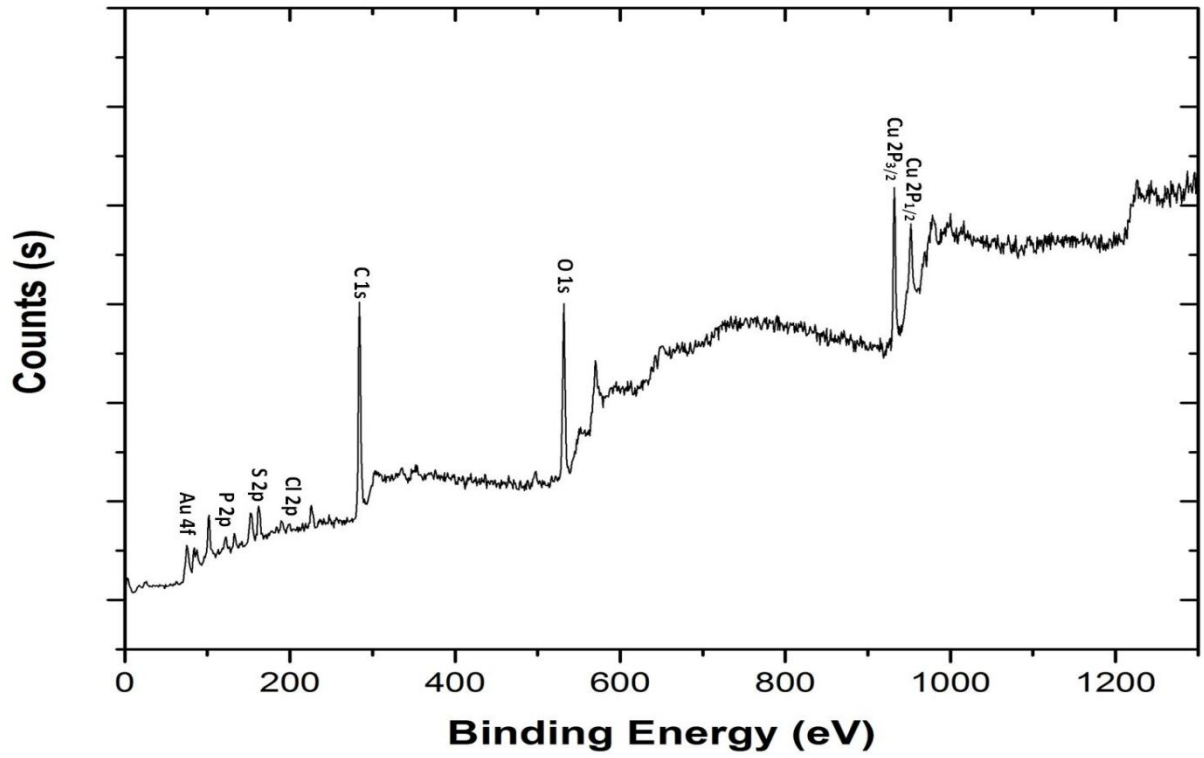

Figure S33. XPS survey spectrum of cluster **2a**. It identifies the presence of gold, copper, sulfur, carbon, nitrogen, and chlorine.

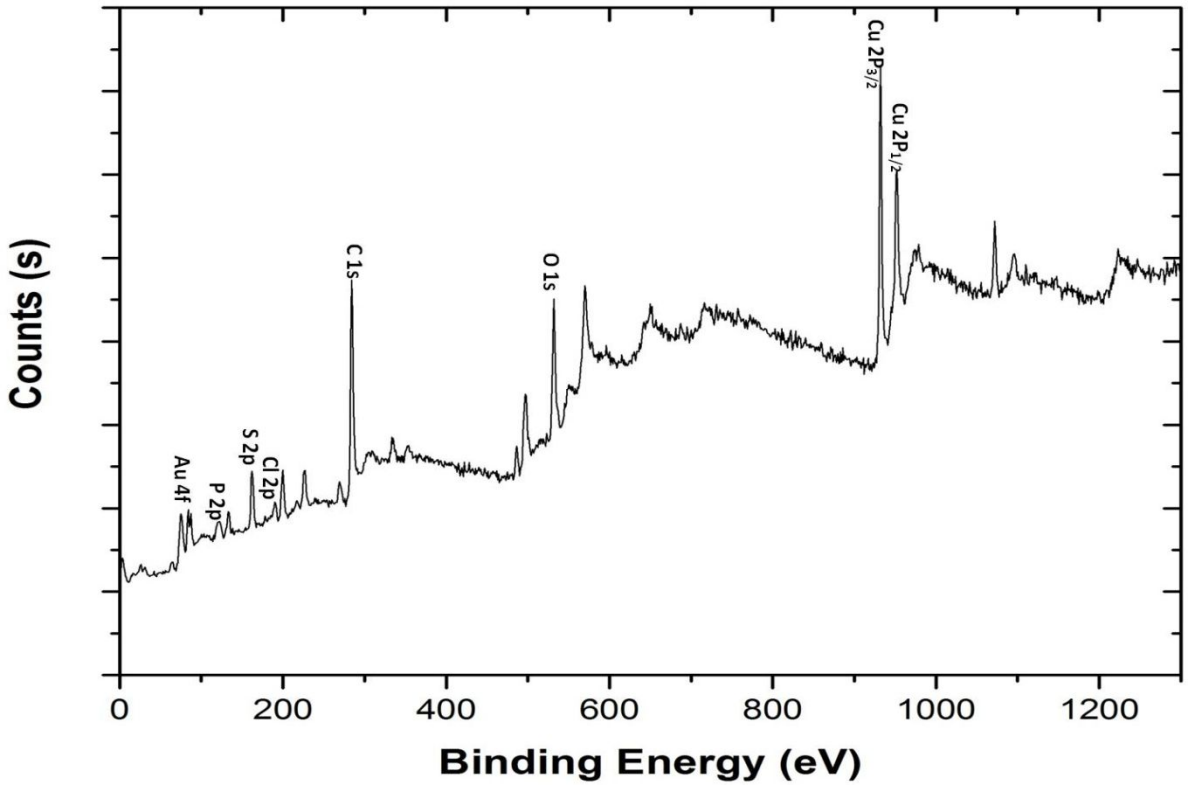

Figure S34. XPS survey spectrum of cluster **2b**. It identifies the presence of gold, copper, sulfur, carbon, nitrogen, and chlorine.

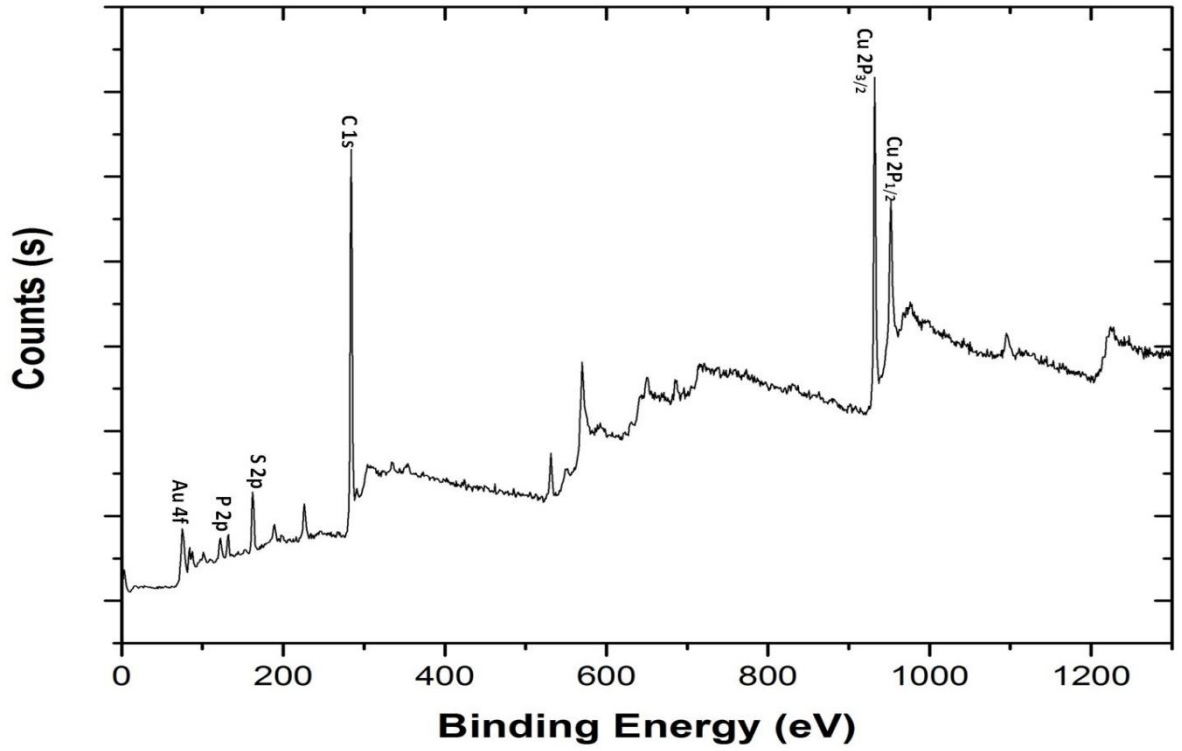

Figure S35. XPS survey spectrum of cluster **2c**. It identifies the presence of gold, copper, sulfur, carbon, nitrogen, and chlorine.

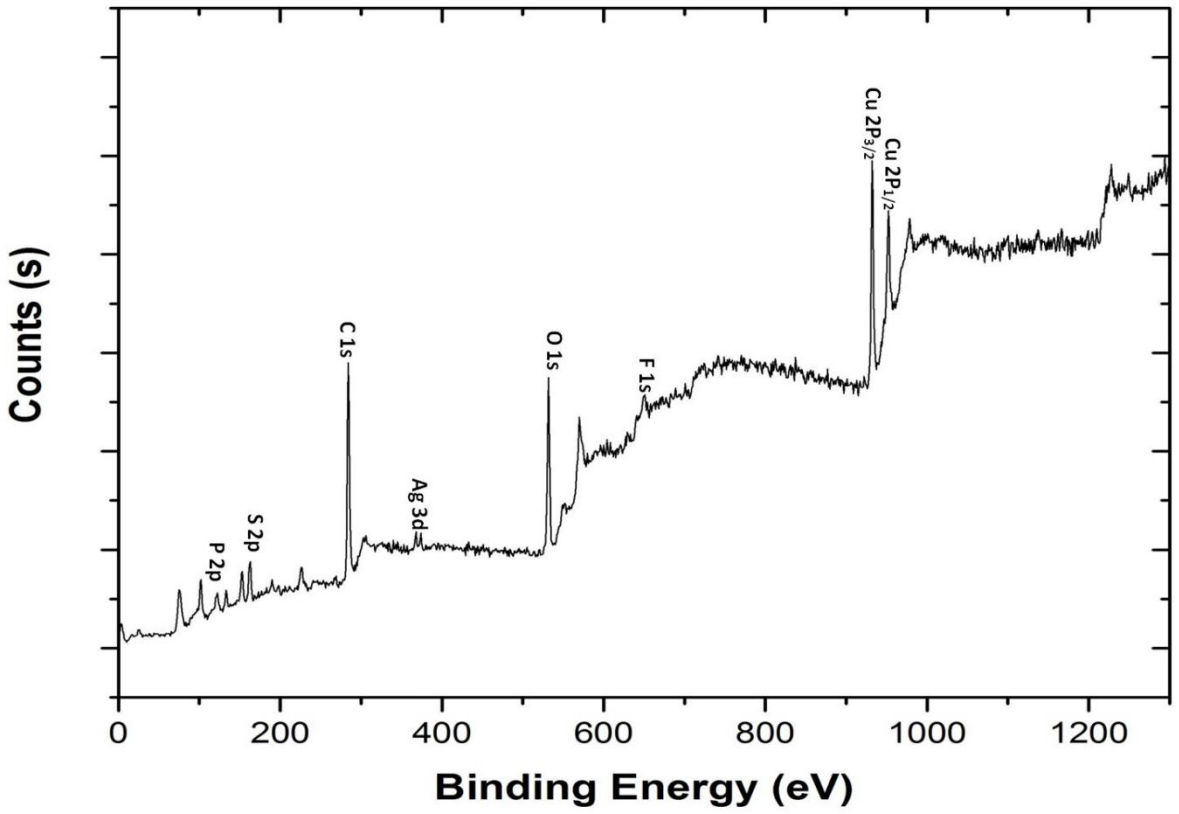

Figure S36. XPS survey spectrum of cluster **3**. It identifies the presence of silver, copper, sulfur, carbon, nitrogen, and chlorine.

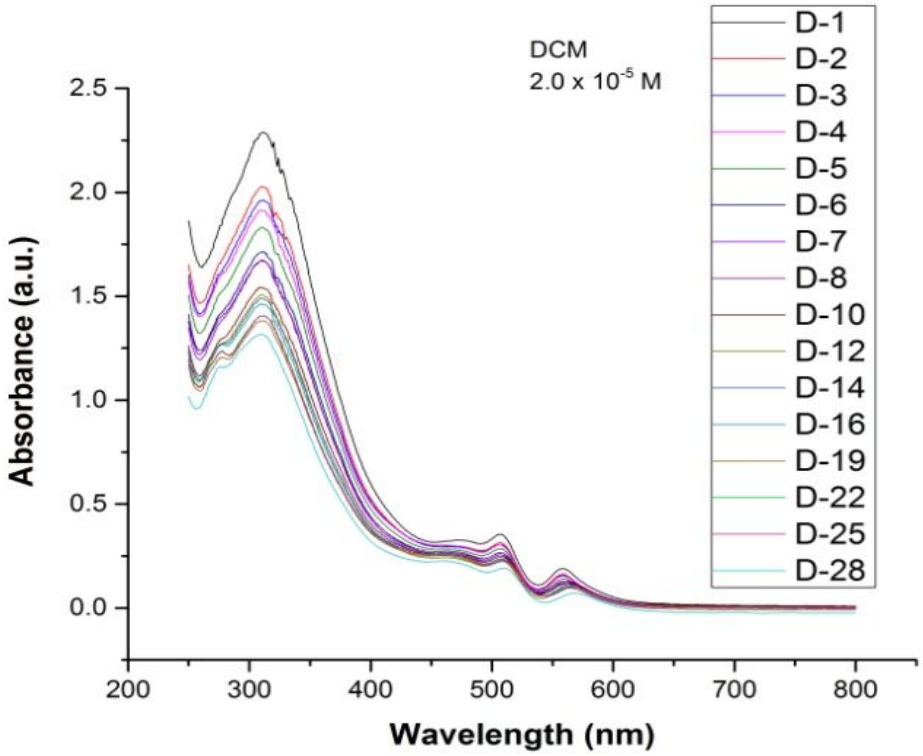

Figure S37. Time-dependent UV-visible spectra for cluster **1a** (295 K, CH_2Cl_2).

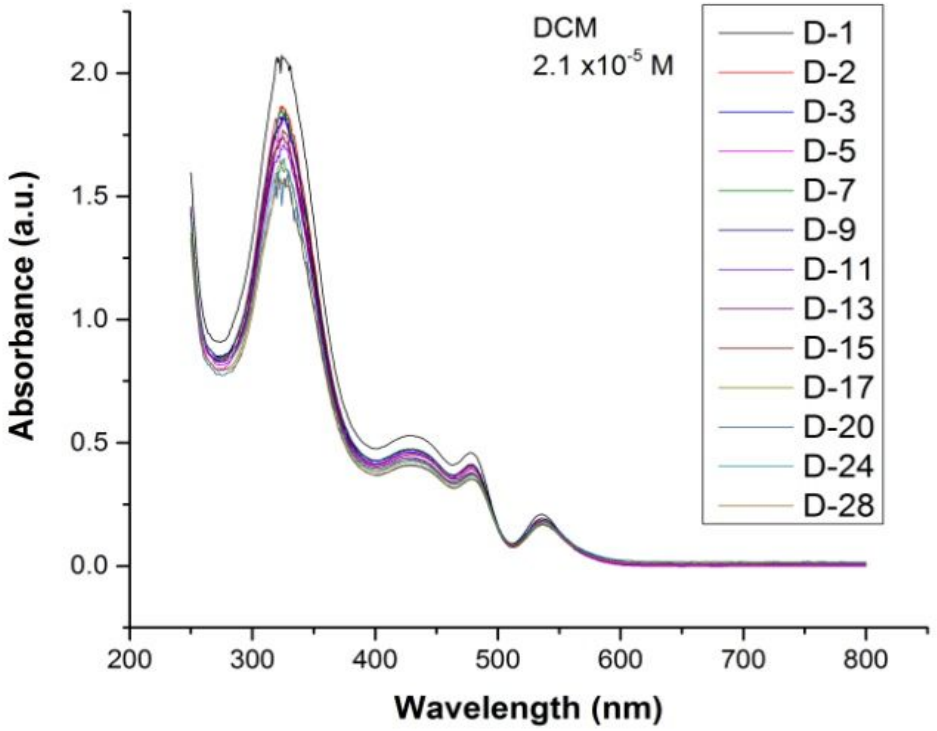

Figure S38. Time-dependent UV-visible spectra for cluster **2a** (295 K, CH_2Cl_2).

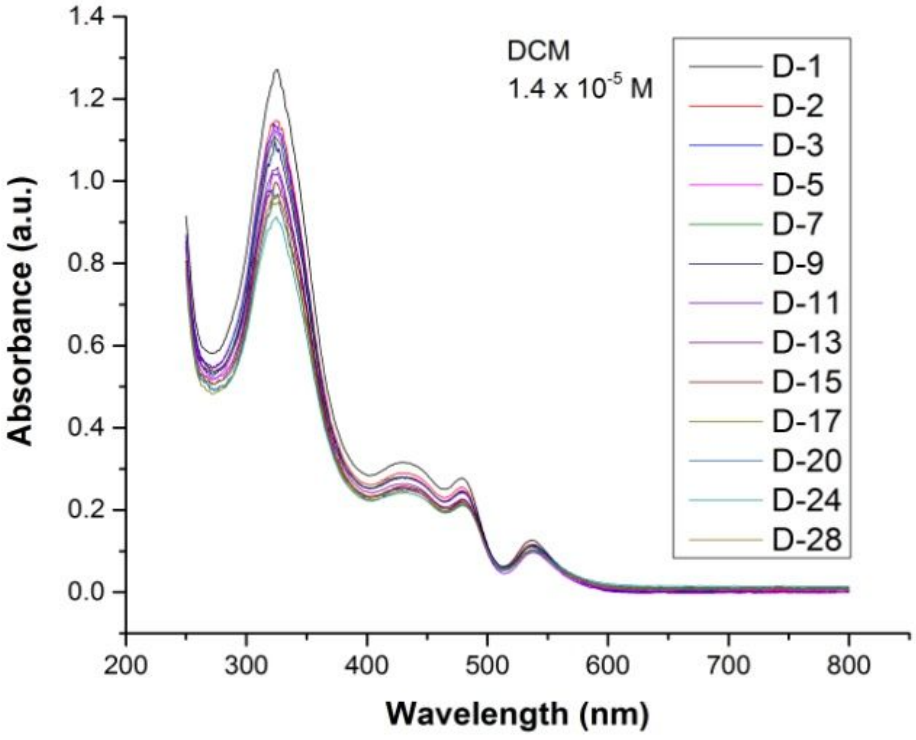

Figure S39. Time-dependent UV-visible spectra for cluster **2b** (295 K, CH_2Cl_2).

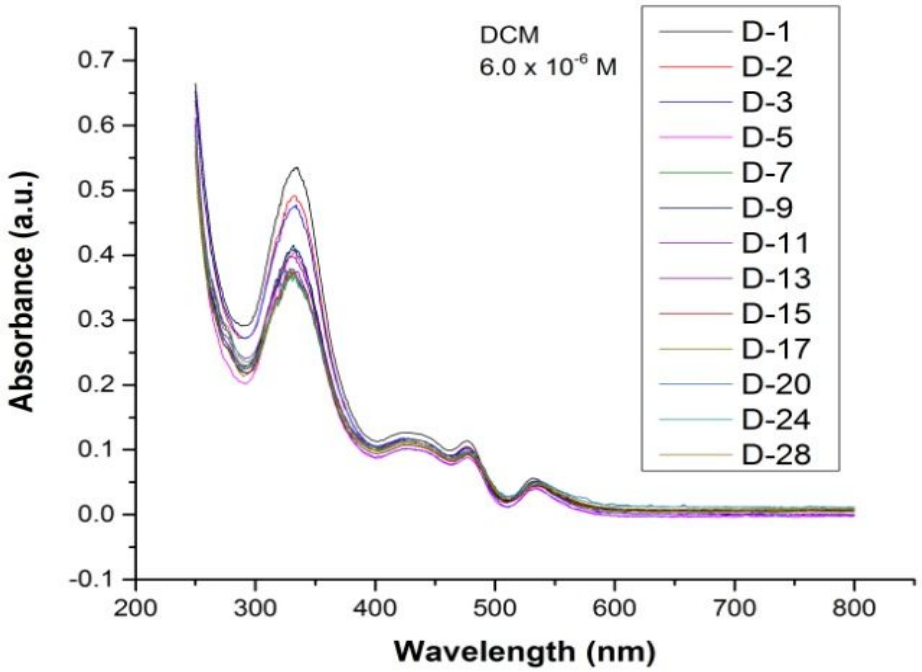

Figure S40. Time-dependent UV-visible spectra for cluster **2c** (295 K, CH_2Cl_2).

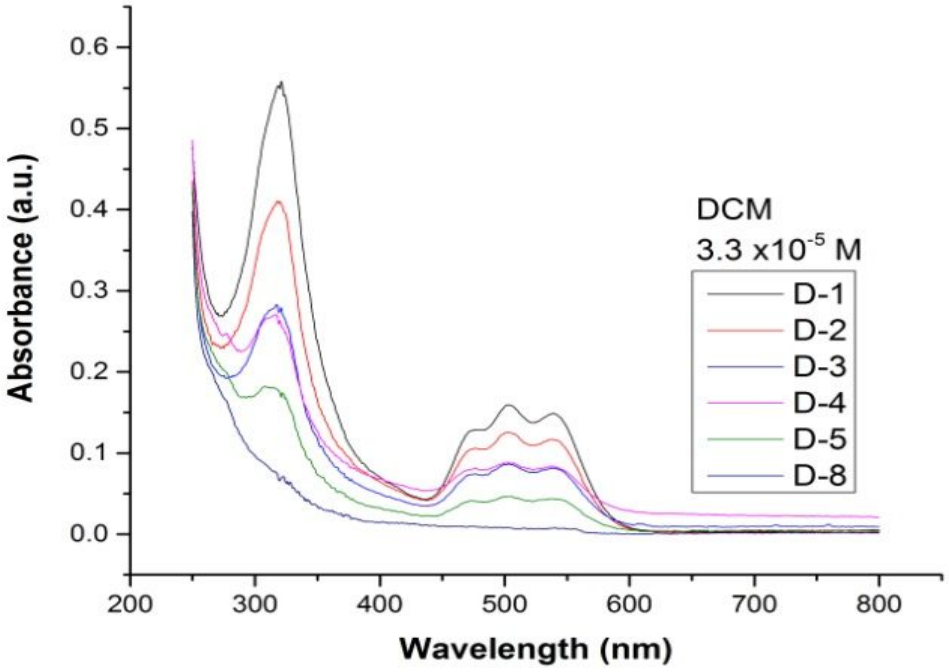

Figure S41. Time-dependent UV-visible spectra for **3** (295 K, CH_2Cl_2).

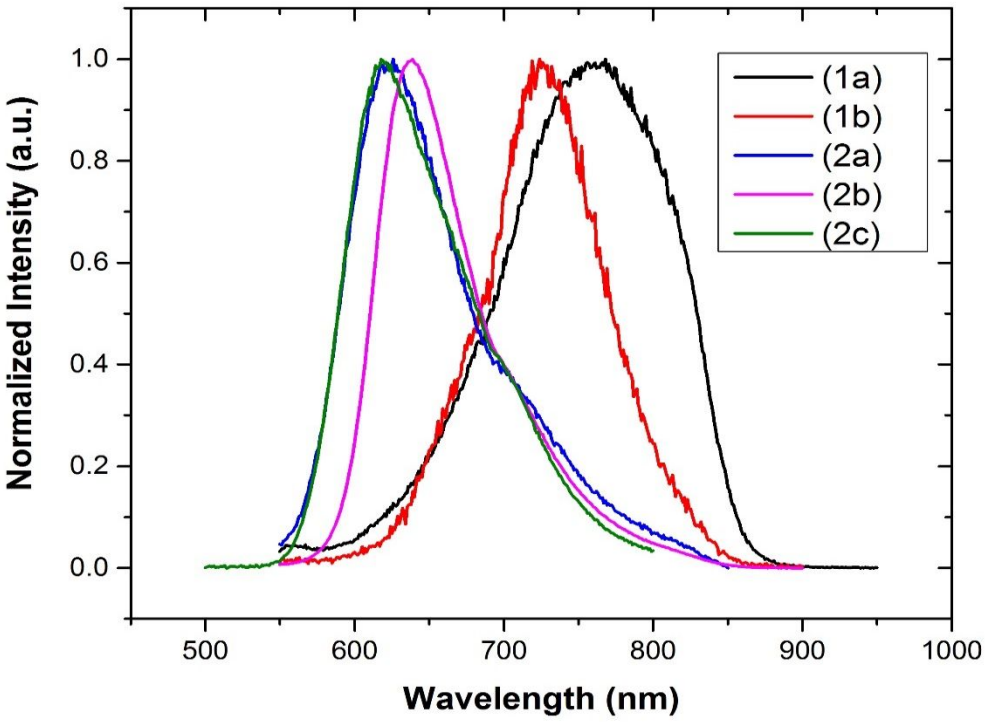

Figure S42. Emission spectra of cluster **1a**, **1b**, **2a**, **2b**, and **2c** in solid state at ambient temperature (λ_{exc} = 473 nm).

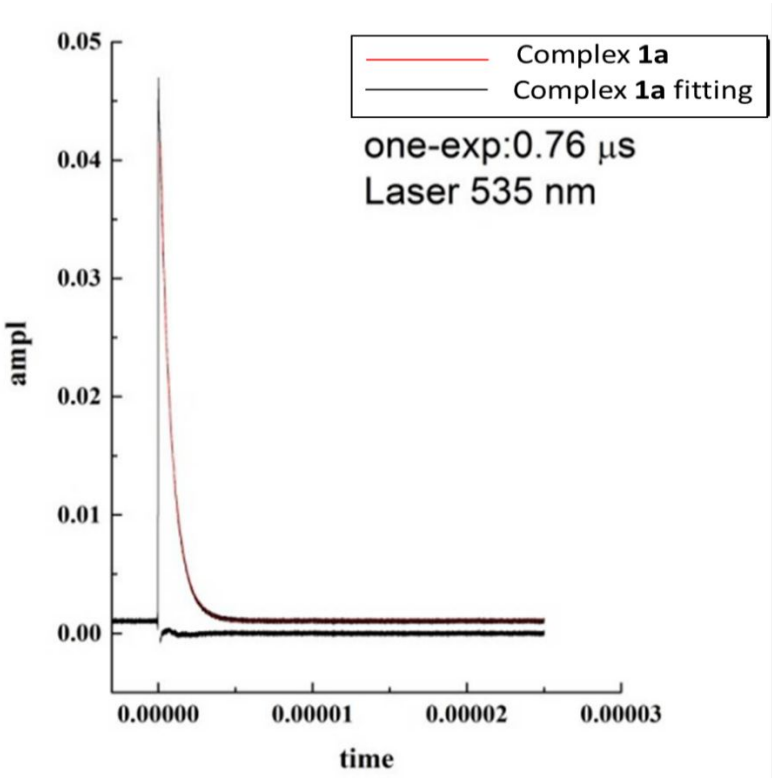

Figure S43. 298K emission lifetime of cluster **1a** in 2-MeTHF. Cluster **1a** was excited at 475 nm.

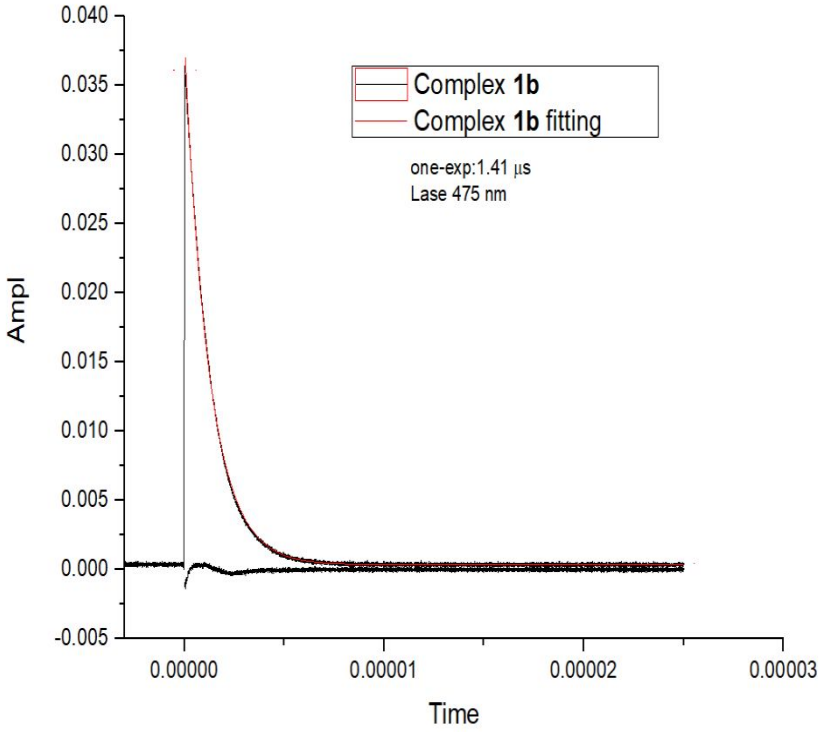

Figure S44. 298K emission lifetime of cluster **1b** in 2-MeTHF. Cluster **1b** was excited at 475 nm.

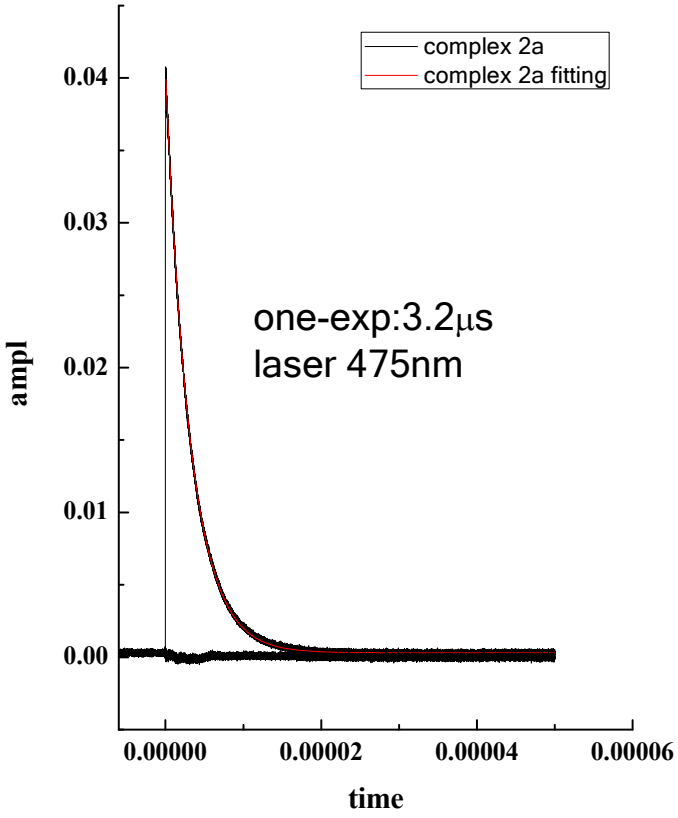

Figure S45. 298K emission lifetime of **2a** in 2-MeTHF. Cluster **2a** was excited at 475 nm.

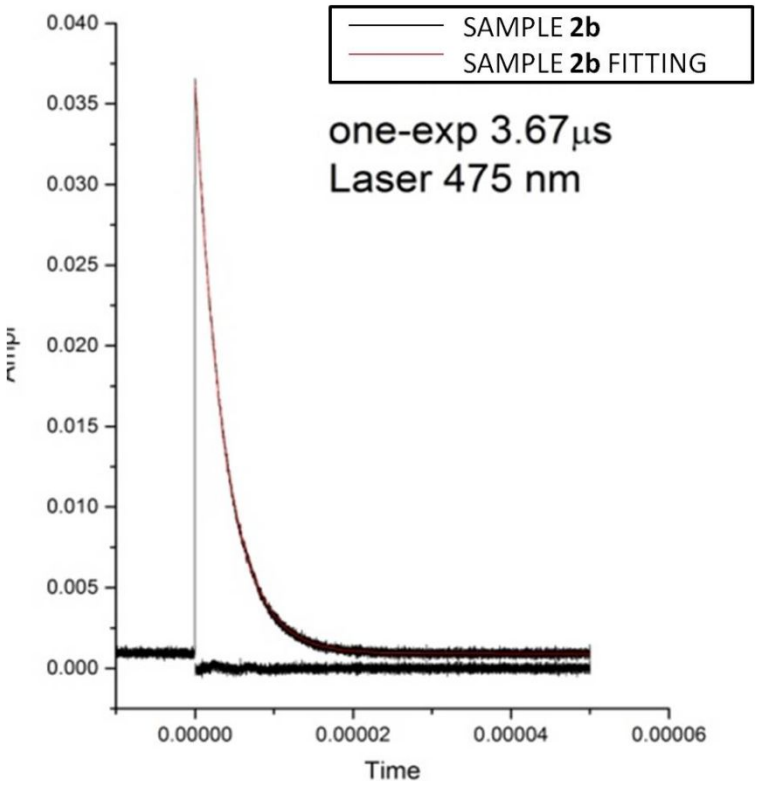

Figure S46. 298K emission lifetime of **2b** in 2-MeTHF. Cluster **2b** was excited at 475 nm.

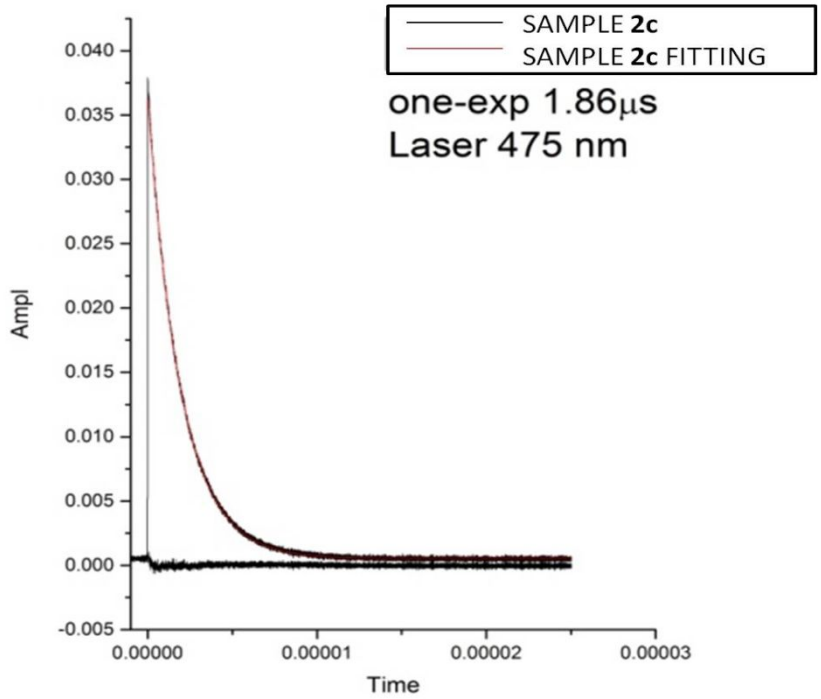

Figure S47. 298K emission lifetime of **2c** in 2-MeTHF. Cluster **2c** was excited at 475 nm.

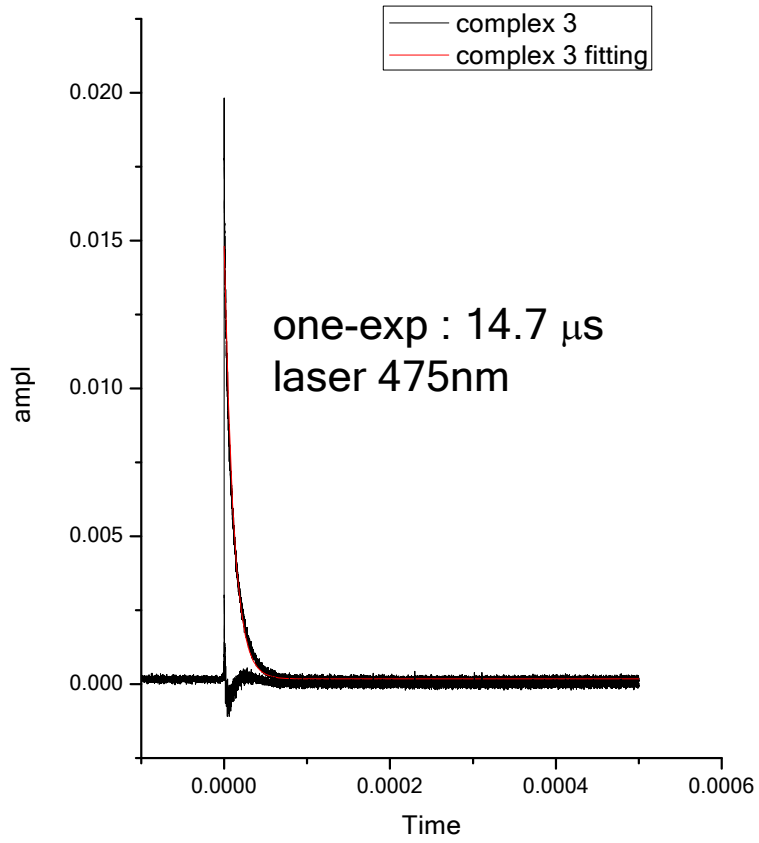

Figure S48. 298K emission lifetime of **3** in 2-MeTHF. Cluster **3** was excited at 475 nm.

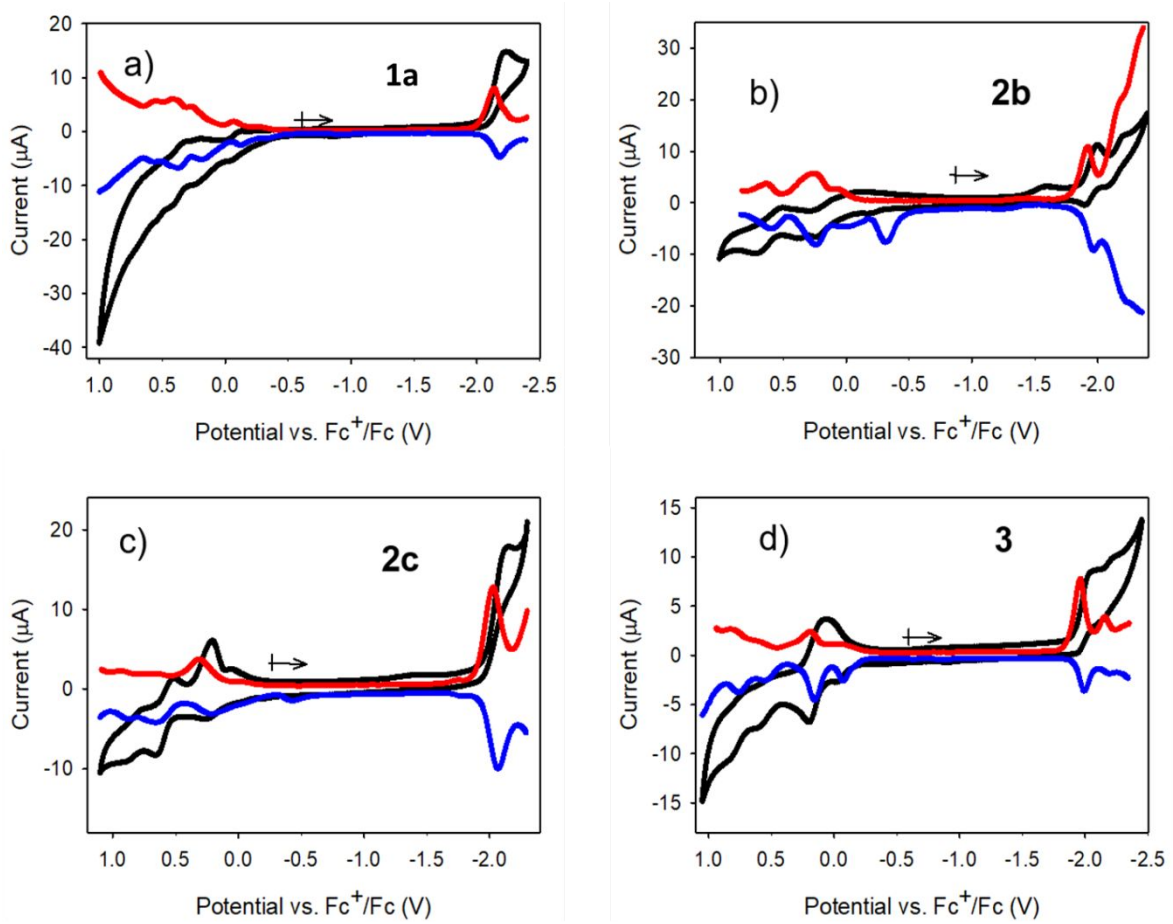

Figure S49. Cyclic voltammogram (black) and differential pulse voltammograms (red and blue) of cluster **1a** (a), **2b** (b), **2c** (c) and **3** (d) at 233 K in CH_2Cl_2 solution under N_2 atmosphere ([**3**] = 0.8 mM, 1 or 3 mm vitreous carbon electrode, 0.1 M [^{n}Bu$_4$N][BArF$_{24}$]. Anodic and cathodic scans of DPVs are displayed in blue and red, respectively; amplitude: 50 mV, pulse period: 0.5 s, pulse width: 50 ms)

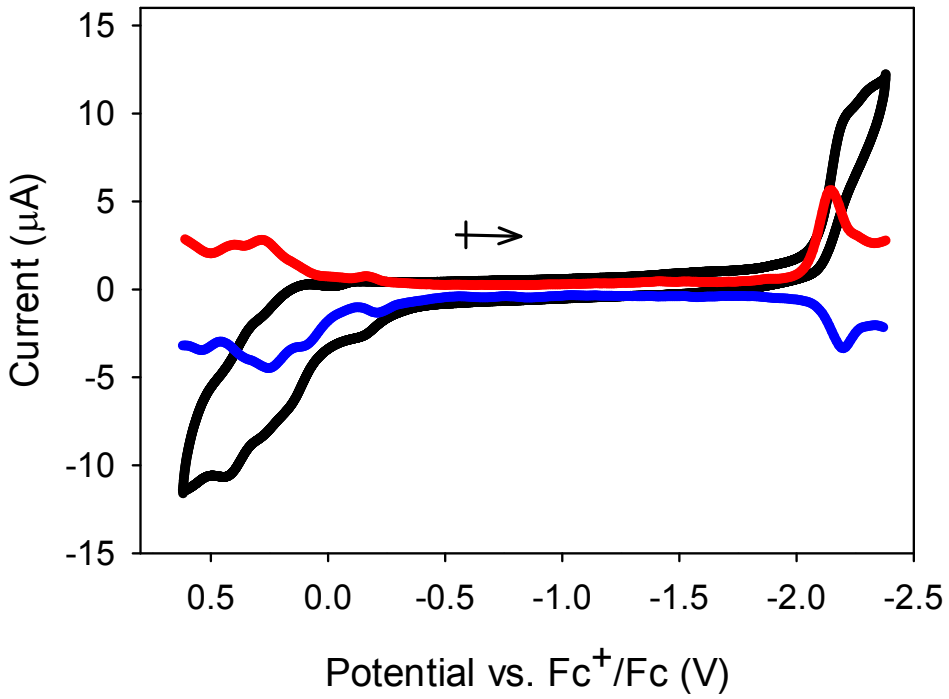

Figure S50. Cyclic voltammogram (black) and differential pulse voltammograms (red and blue) of $[AuCu_{12}\{S_2CN^nBu_2\}_6(C_2Ph)_4]^+$ at 233 K in CH_2Cl_2 solution under N_2 atmosphere (3 mm vitreous carbon electrode, 0.1 M $[^nBu_4N][B(C_6F_5)_4]$. Anodic and cathodic scans of DPVs are displayed in blue and red, respectively; amplitude: 50 mV, pulse period: 0.5 s, pulse width: 50 ms)

Table S1. Selected crystallographic data of **1a**, **2a**, **2b**, and **3**.

	1a	**2a**	**2b**	**3**
CCDC number	2022342	2022343	2022344	2022345
Empirical formula	$C_{74}H_{104}AuCl_2Cu_{13}N_6S_{12}$	$C_{68}H_{104}AuCl_2Cu_{13}O_{12}P_6S_{12}$	$C_{68}H_{104}AuClCu_{12}O_{12}P_6S_{12}$	$C_{68}H_{104}AgCu_{12}F_6O_{12}P_7S_{12}$
Formula weight	2556.23	2777.93	2678.94	2699.37
Temperature, K	150(2)	150(2)	150(2)	150(2)
Wavelength, Å	0.71073	0.71073	0.71073	0.71073
Crystal system	Monoclinic	Monoclinic	Triclinic	Monoclinic
Space group	$P2_1/c$	$P2_1/n$	P(-)1	$P2_1/n$
a, Å	15.967(5)	19.0932(11)	17.2411(6)	18.4252(4)
b, Å	36.869(12)	27.0410(16)	17.9160(6)	23.5477(5)
c, Å	16.500(5)	19.1086(12)	18.2922(6)	22.5694(5)
α, deg.	90	90	87.9830(10)	90
β , deg.	103.270(12)	98.0105(15)	66.1590(10)	90.4479(6)
γ , deg.	90	90	66.1120(10)	90
Volume, $Å^3$	9454(5)	9769.5(10)	4669.4(4)	9791.9(4)
Z	4	4	2	4
Calculated density, Mg m^{-3}	1.796	1.889	1.905	1.831
Absorption coefficient, mm^{-1} (neutron, cm^{-1})	4.765	4.720	4.687	3.175
Crystal size, mm^3	0.120 x 0.110 x 0.050	0.200 x 0.100x 0.030	0.160x 0.130 x 0.060	0.110x 0.100 x 0.050
θ_{max}, deg.	27.125	25.079	24.999	27.319
Reflections collected / unique	84053/ 20828 (R_{int} = 0.0495)	71415 /17320 (R_{int} = 0.0465)	28895/ 16193 (R_{int} = 0.0213)	58888 / 22024 (R_{int} = 0.0304)
Completeness, %	99.7	99.7	98.5	99.7
restraints / parameters	456/ 984	563 / 1087	570/ 1066	329 / 1085
GºF	1.070	1.065	1.067	1.031
Final R indices [I>2σ(I)]	R1 = 0.0516, wR2 = 0.1059	R1 = 0.0519, wR2 = 0.1251	R1 = 0.0576, wR2 = 0.1588	R1 = 0.0419, wR2 = 0.0977
R indices (all data)	R1 = 0.0870, wR2 = 0.1233	R1 = 0.0840, wR2 = 0.1474	R1 = 0.0827, wR2 = 0.1820	R1 = 0.0708, wR2 = 0.1152
Largest diff. peak / hole, e $Å^{-3}$ (neutron, fm)	1.688, -1.896	1.711, -1.717	2.015, -1.066	1.468, -1.144

References

1. Tsai, C. N.; Mazumder, S.; Zhang, X. Z.; Schlegel, H. B.; Chen, Y. J.; Endicott, J. F. Are Very Small Emission Quantum Yields Characteristic of Pure Metal-to-Ligand Charge-Transfer Excited States of Ruthenium(II)-(Acceptor Ligand) Chromophores? *Inorg. Chem*. **2016**, 55, 7341-7355.
2. Tsai, C. N.; Tian, Y.-H.; Shi, X.; Lord, R. L.; Schlegel, H. B.; Chen, Y. J.; Endicott, J. F. Experimental and DFT Characterization of Metal-to-Ligand Charge-Transfer Excited States of (Rutheniumammine)(Monodentate Aromatic Ligand) Chromophores. *Inorg. Chem*. **2013**, *52*, 9774-9790.
3. Tsai, C. N.; Mazumder, S.; Zhang, X. Z.; Schlegel, H. B.; Chen, Y. J.; Endicott, J. F. Metal-to-Ligand Charge-Transfer Emissions of Ruthenium(II) Pentaammine Complexes with Monodentate Aromatic Acceptor Ligands and Distortion Patterns of their Lowest Energy Triplet Excited States. *Inorg. Chem*. **2015**, *54*, 8495-8508.
4. Thomas, R. A.; Tsai, C. N.; Mazumder, S.; Lu, I. C.; Lord, R. L.; Schlegel, H. B.; Chen, Y. J.; Endicott, J. F. Energy Dependence of the Ruthenium(II)-Bipyridine Metal-to-Ligand-Charge-Transfer Excited State Radiative Lifetimes: Effects of ππ*(bipyridine) Mixing. *J. Phys. Chem. B*. **2015**, *119*, 7393-7406.
5. Cook, M. J.; Lewis, A. P.; McAuliffe, G. S. G.; Skarda, V.; Thomson, A. J.; Glasper, J. L.; Robbins, D. J. Luminescent metal complexes. Part 1. Tris-chelates of substituted 2,2′-bipyridyls with ruthenium (II) as dyes for luminescent solar collectors. *J. Chem. Soc. Perkin Trans*. *2*. **1984**, *8*, 1293-1301.
6. Demas, J. N.; Crosby, G. A. Quantum efficiencies of transition-metal complexes. I. d-d Luminescence. *J. Am. Chem. Soc*. **1970**, *92*, 7262-7270.
7. Demas, J. N.; Crosby, G. A. Quantum efficiencies on transition metal complexes. II. Charge-transfer luminescence. *J. Am. Chem. Soc*. **1971**, *93*, 2841-2847.
8. Ravi Kishore, V. V. N.; Narasimhan, K. L.; Periasamy, N. On the radiative lifetime, quantum yield and fluorescence decay of Alq in thin films. *Phys. Chem. Chem. Phys*. **2003**, *5*, 1386-1391.
9. Zoon, P. D.; Brouwer, A. M. A push-pull aromatic chromophore with a touch of merocyanine. *Photochem. Photobiol*. **2009**, *8*, 345-353.